

UNDERSTANDING RESERVOIR ENGINEERING ASPECTS OF SHALE OIL  
DEVELOPMENT ON THE ALASKA NORTH SLOPE

By

Behnam Zanganeh

RECOMMENDED:



Dr. Obadare Awoleke  
Advisory Committee Member



Dr. Catherine Hanks  
Advisory Committee Co-Chair



Dr. Mohabbat Ahmadi  
Advisory Committee Co-Chair

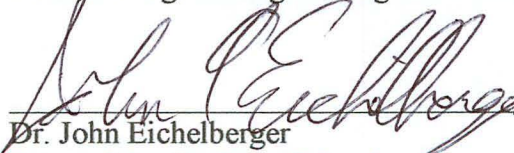


Dr. Abhijit Dandekar,  
Chair, Department of Petroleum Engineering

APPROVED:



Dr. Douglas Goering  
Dean, College of Engineering and Mines



Dr. John Eichelberger  
Dean of the Graduate School

4/21/14

Date



UNDERSTANDING RESERVOIR ENGINEERING ASPECTS OF SHALE OIL  
DEVELOPMENT ON THE ALASKA NORTH SLOPE

A  
THESIS

Presented to the Faculty  
of the University of Alaska Fairbanks

in Partial Fulfillment of the Requirements  
for the Degree of

MASTER OF SCIENCE

By

Behnam Zanganeh, B.S.

Fairbanks, Alaska

May 2014

## Abstract

Horizontal drilling and multi-stage hydraulic fracturing have made the commercial development of nano-darcy shale resources a success. The Shublik shale, a major source rock for hydrocarbon accumulations on the North Slope of Alaska, has huge potential for oil and gas production, with an estimated 463 million barrels of technically recoverable oil.

This thesis presents a workflow for proper modeling of flow simulation in shale wells by incorporating results from hydraulic fracturing software into hydraulic fracture flow modeling. The proposed approach allows us to simulate fracture propagation and leak-off of fracturing fluid during hydraulic fracturing. This process honors the real proppant distribution, horizontal and vertical variable fracture conductivity, and presence of fracturing fluid in the fractures and surrounding matrix. Data from the Eagle Ford Shale in Texas was used for this modeling which is believed to be analogous to Alaska's Shublik shale.

The performance of a single hydraulic fracture using a black oil model was simulated. Simulation results showed that for the hydraulically fractured zone, the oil recovery factor is 5.8% over thirty years of production, to an assumed economic rate of 200 STB/day. It was found that ignoring flowback overestimated oil recovery by about 17%. Assuming a constant permeability in the hydraulic fracture plane resulted in overestimation of oil recovery by almost 25%. The conductivity of the unpropped zone affected the recovery factor predictions by as much as 10%. For the case investigated, about 25% of the fracturing fluid was recovered during the first 2 months of production; in total, 44% of it was recovered over thirty years. Permeability anisotropy was found to have a significant effect on the results.

These results suggest that assuming a constant conductivity for the fractures and ignoring the presence of water in the fractures and the surrounding matrix leads to overestimation of initial production rates and final recovery factors. In addition, the modified workflow

developed here more accurately and seamlessly integrates the modeled induced fracture characteristics in the reservoir simulation of shale resource plays.

Dedicated to:

My Mother and My Wife



## **Acknowledgments**

I would like to thank my committee chair, Dr. Ahmadi, for his support, technical suggestions, and guidance during the course of this research. I also would like to acknowledge my committee members, Dr. Hanks and Dr. Awoleke, for their feedback, help, and support.

I would like to extend my gratitude to Dr. Dandekar and Dr. Patil for their support during my studies at UAF. Thanks also go to the department faculty and staff and my friends and colleagues for making my time at UAF a great experience. Special thanks go to my friends Iman Oraki and Vahid Nourpour.

I would like to acknowledge the Alaska Department of Natural Resources for supporting the project and Computer Modeling Group (CMG) and CARBO for providing CMG and Fracpro software.

Last but not the least, I would like to express my heartfelt gratitude to my mother and my wife for their encouragement, patience, and love.





## Table of Contents

<b>Signature Page .....</b>	<b>i</b>
<b>Title Page .....</b>	<b>iii</b>
<b>Abstract.....</b>	<b>v</b>
<b>Dedication .....</b>	<b>vii</b>
<b>Acknowledgments .....</b>	<b>ix</b>
<b>Table of Contents .....</b>	<b>xi</b>
<b>List of Figures.....</b>	<b>xv</b>
<b>List of Tables .....</b>	<b>xxi</b>
<b>Chapter 1 Introduction.....</b>	<b>1</b>
1.1 Overview .....	1
1.2 Objective .....	4
<b>Chapter 2 Literature Review .....</b>	<b>5</b>
2.1 U.S. Shale Plays .....	5
2.2 Description of Shublik Formation.....	8
2.2.1 Subsurface Shublik Formation Stratigraphy.....	8
2.2.2 Shublik Formation Potential as a Shale Resource Play .....	11
2.3 Description of the Eagle Ford Shale .....	16

2.3.1	Eagle Ford Shale Geology .....	16
2.3.2	Eagle Ford Shale Mineralogy .....	18
2.3.3	Petrophysical Properties of the Eagle Ford.....	19
2.3.4	PVT Behavior in the Eagle Ford Shale.....	21
2.3.5	The Eagle Ford Shale as a Possible Analog for the Shublik Shale.....	25
2.4	Hydraulic Fracturing .....	28
2.4.1	Propped Zone and Unpropped Zone .....	30
2.4.2	Environmental Concerns of Hydraulic Fracturing and Wastewater Production.....	31
2.5	Modeling of Shale Reservoirs .....	34
2.6	Description of Simulators.....	36
<b>Chapter 3</b>	<b>Methodology and Model Construction .....</b>	<b>37</b>
3.1	Hydraulic Fracture Design .....	38
3.2	Model I Description .....	42
3.2.1	Simulation Parameters .....	45
3.2.2	Fluid Model.....	46
3.2.3	Relative Permeability Curves .....	48
3.2.4	Fracture Closure.....	52
3.3	Model II.....	53

3.3.1	Incorporating Fracpro Results into the CMG-IMEX.....	54
<b>Chapter 4</b>	<b>Results and Discussion.....</b>	<b>59</b>
4.1	Model I.....	59
4.1.1	Effect of Matrix Porosity and Permeability .....	61
4.1.2	Effect of Hydraulic Fracture Permeability.....	64
4.1.3	Effect of Fracture Closure.....	65
4.2	Model II.....	66
4.2.1	Injection Profiles during Treatment .....	66
4.2.2	Production Trends.....	67
4.2.3	Effect of Fracturing Fluid Flowback.....	69
4.2.4	Fracturing Fluid Recovery .....	71
4.2.5	Effect of Unpropped Zone Conductivity on Production Performance .....	73
4.2.6	Effect of Hydraulic Fracture Conductivity Profile on Production Performance .....	74
4.2.7	Effect of Permeability Anisotropy .....	75
<b>Chapter 5</b>	<b>Conclusions and Recommendations.....</b>	<b>77</b>
5.1	Conclusions .....	77
5.2	Recommendations .....	78
<b>References</b>	<b>.....</b>	<b>81</b>



## List of Figures

Figure 1: The concept of resource triangle for conventional and unconventional oil and gas resources. ....	2
Figure 2: Graphical definition of unconventional reservoirs based on reservoir permeability and fluid viscosity.....	3
Figure 3: U.S. shale gas and shale oil plays.....	5
Figure 4: Typical lithostratigraphy and corresponding gamma ray log response for the Eileen Sandstone, Shublik Formation, and Sag River Sandstone based on the wells in and around Prudhoe Bay.....	10
Figure 5: Map of Northern Alaska showing lithologic facies of Shublik Formation. ....	11
Figure 6: Generalized North-South cross section across the Central North Slope of Alaska. The stratigraphic position of Shublik is shown schematically by the pink line. Generalized thermal maturity zones are shown by the broad dashed green and red lines; source rocks are immature above the green line, are in the oil window between the green and red lines, and are in the gas window below and south of the red line.....	12
Figure 7: Map of Northern Alaska showing the thickness of oil-prone part of Shublik Formation and extent of Shublik shale oil (outlined in black) and shale gas (outlined in red dashes). ....	13
Figure 8: USGS estimates of undiscovered oil, showing the potential of the North Slope in comparison to major U.S. shale oil plays. ....	15

Figure 9: Eagle Ford Shale play..... 16

Figure 10: Upper Cretaceous stratigraphic column showing the Eagle Ford Shale. .... 17

Figure 11: Eagle Ford Shale mineralogy. .... 19

Figure 12: Eagle Ford petrophysical properties plotted against depth. .... 20

Figure 13: Fluid type variations in the Eagle Ford Shale. .... 22

Figure 14: Description of the hydraulic fracturing process. .... 29

Figure 15: (a) Horizontal well with high conductivity hydraulic fractures. (b) Horizontal well with hydraulic fractures in a naturally fractured formation. .... 30

Figure 16: Vertical proppant distribution in a hydraulic fracture. .... 31

Figure 17: Modification of hydraulic fracture with porosity modifier. .... 35

Figure 18: 2-D schematic of a multistage hydraulically fractured horizontal well in a shale reservoir. The zone separated with blue dashed lines is chosen for reservoir simulation..... 38

Figure 19: Fracture propagation stages generated by Fracpro..... 41

Figure 20: (a) 2-D top view of middle layer in single hydraulic fracture model. b) 3-D view of single hydraulic fracture model. .... 43

Figure 21: Side view of simulation model at fracture plane; matrix blocks and hydraulic fracture blocks are represented by blue and green colors, respectively.....	44
Figure 22: Oil formation volume factor ( $B_o$ ) and solution gas oil ratio ( $R_s$ ) as a function of pressure.....	47
Figure 23: Oil viscosity trend versus pressure.....	47
Figure 24: (a) Water-oil relative permeability curve for TOC-rich matrix. (b) Liquid-gas relative permeability curve for TOC-rich matrix.....	50
Figure 25: (a) Water-oil relative permeability curve for hydraulic fracture blocks. (b) Liquid-gas relative permeability curve for hydraulic fracture blocks. ....	51
Figure 26: Pressure-dependent permeability multipliers for hydraulic fracture blocks. ..	52
Figure 27: Conceptual model of flowback before and after breakthrough of formation fluid. (a) Fracturing fluid (blue arrows) production at early production time. (b) Breakthrough of formation fluid (green arrows). ....	53
Figure 28: Side view of half of Model II at the fracture plane after fracture propagation stages imported into the reservoir simulation software. Red blocks represent hydraulic fracture and blue blocks represent matrix. At each stage water is injected into the model according to the pumping schedule.....	55
Figure 29: Side view of simulation models showing permeability distribution at the start of production. (a) Model II, where the permeability distribution is based on the last stage of hydraulic fracturing. (b) Model I, where permeability in fracture blocks remains constant, equal to the average values shown in (a).....	56



Figure 30: Oil production rate and cumulative oil production for Model I. .... 59

Figure 31: Producing GOR and average reservoir pressure for Model I during production time. .... 60

Figure 32: (a) Effect of matrix porosity on oil in place and recovery factor in Model I. (b) Oil production rate and cumulative oil production versus time when minimum production rate constraint is used. (c) Oil recovery factor versus cumulative oil production when minimum production rate constraint is used. .... 62

Figure 33: Effect of matrix permeability on oil recovery factor in Model I. .... 63

Figure 34: Effect of hydraulic fracture permeability on oil recovery factor in Model I.. 64

Figure 35: Effect of fracture closure during depletion on oil recovery factor in Model I. 65

Figure 36: Water injection profile in Model II. .... 66

Figure 37: Oil and water production trends during 30 years of production in Model II. . 67

Figure 38: Oil and water production trends during first year of production in Model II. 68

Figure 39: Cumulative oil production and recovery factor for Model II. .... 68

Figure 40: Oil production trend with and without considering fracturing fluid (water) flowback in Model II. .... 70

Figure 41: Comparison of cumulative oil production with and without considering fracturing fluid (water) flowback in Model II. .... 70

Figure 42: Amount of recovered fracturing fluid (water) during 30 years of production time in Model II. .... 71

Figure 43: Recovered fracturing fluid (water) during the first year of production as a percentage of total recovery during 30 years. .... 72

Figure 44: Effect of unpropped zone permeability on the oil recovery factor in Model II. .... 73

Figure 45: Comparison of oil recovery factor for two approaches in modeling of fracture conductivity/permeability in Model II. .... 74

Figure 46: Effect of permeability anisotropy on production performance in Model II. ... 75



## List of Tables

Table 1: INTEK estimates of undeveloped technically recoverable shale gas and shale oil resources remaining in discovered shale plays as of January 1, 2009. ....	7
Table 2: USGS Shublik Formation shale oil and shale gas assessment results. ....	14
Table 3: North Slope potential compared to other U.S. shale plays. ....	15
Table 4: Minerals identified in the Eagle Ford Shale. ....	18
Table 5: Average values for petrophysical properties of two petrotypes identified in the Eagle Ford oil window. ....	21
Table 6: Molar composition of synthetic Eagle Ford oil. ....	23
Table 7: Molar composition of synthetic Eagle Ford gas condensates. ....	24
Table 8: Black oil PVT properties for the Eagle Ford oil window. ....	25
Table 9: Similar characteristics of the Eagle Ford Shale and the Shublik shale. ....	26
Table 10: Reservoir simulation parameters. ....	27
Table 11: Summary of mechanical properties used for fracturing design simulation. ....	39
Table 12: The typical slickwater pumping schedule of hydraulic fracturing. ....	40
Table 13: Model I reservoir simulation parameters. ....	45

Table 14: Reservoir fluid properties. ....	46
Table 15: Relative permeability models for the Eagle Ford.....	49
Table 16: Comparison of Model I and Model II.....	57

## Chapter 1 Introduction

### 1.1 Overview

Conventional reservoirs can produce economic volumes of oil and gas without requiring stimulation treatments or special recovery techniques, although well stimulation is often used to enhance their productivity. According to Holditch (2003), a ‘conventional’ reservoir is a high to medium permeability reservoir in which wells can produce at economic flow rates after drilling operations. On the other hand, ‘unconventional’ reservoirs require massive stimulation treatment or special recovery processes to produce at economic flow rates. Types of unconventional reservoirs include tight-gas sand, coalbed methane, heavy oil, shale gas, shale oil, gas hydrates, and oil shale (Holditch, 2003).

Masters (1979) presented the concept of the resource triangle, which states that similar to natural resources such as gold and copper, oil and gas resources are distributed log-normally in nature. Figure 1 presents this concept, modified by Chaudhary (2011), to distinguish between shale gas and shale oil resources. Conventional resources, which are easy to develop, are located at the top of the triangle. Unconventional resources, which are much more difficult to develop, are located at the bottom of the triangle. The volumes of oil and gas stored in these unconventional resources are significantly higher than the volumes of oil and gas found in conventional resources. Increasingly more advanced technologies, and subsequent higher costs are required to develop oil and gas resources as one moves from the top of the resource triangle to the bottom (Chaudhary, 2011).

Cander (2012) stated that defining unconventional reservoirs based only on permeability threshold ( $<0.1$  md (millidarcy)) is insufficient, due to the fact that many unconventional reservoirs, such as some coalbed methane plays or heavy oil reservoirs, have permeabilities exceeding 1 md. He proposed a graph of viscosity ( $\mu$ ) versus permeability ( $k$ ) for definition of unconventional resources (Figure 2). This definition includes both low and high permeability reservoirs with both low and high viscosity fluids. Based on

Cander's graph, unconventional resources are defined as hydrocarbon reservoirs whose permeability/viscosity ratio requires use of technology to either increase rock permeability or decrease fluid viscosity to achieve production at commercial flow rates.

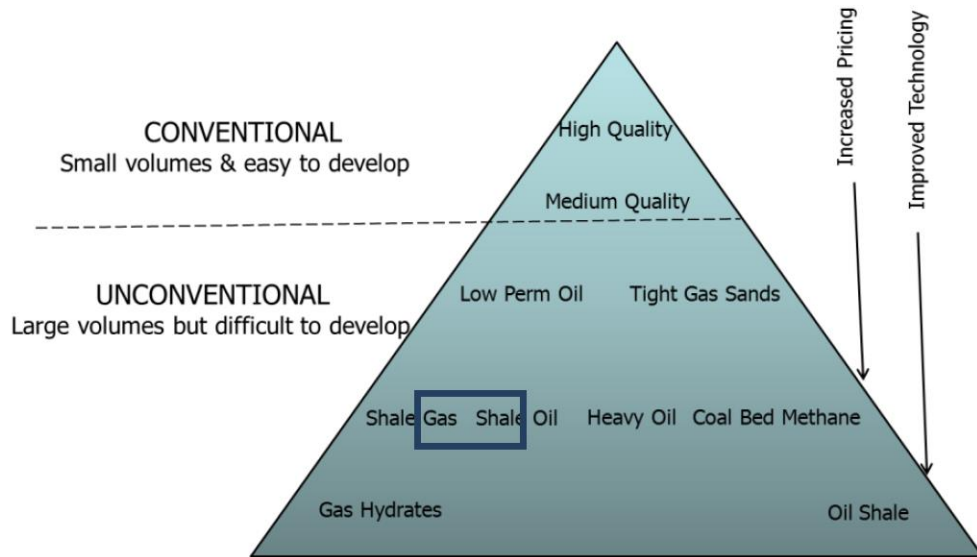


Figure 1: The concept of resource triangle for conventional and unconventional oil and gas resources (Masters, 1979; modified by Chaudhary, 2011).

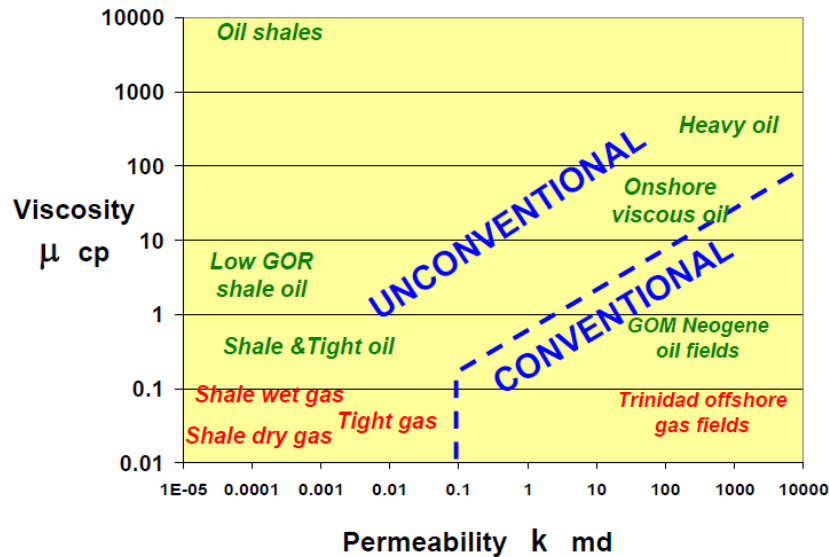


Figure 2: Graphical definition of unconventional reservoirs based on reservoir permeability and fluid viscosity (Cander, 2012).

Shale formations traditionally are regarded as potential source rocks and/or cap rocks for conventional hydrocarbon reservoirs due to their (potentially) high organic content and low permeability, respectively. Recently, shales have been recognized as potential reservoirs for hydrocarbons, despite their much lower permeability compared to conventional reservoir rocks. The low permeability of shale reservoirs requires special completion techniques to enable commercial production. Recent advances in horizontal drilling and multistage hydraulic fracturing have made natural gas and oil production from low permeability formations, particularly shale plays, a reality.



## 1.2 Objective

United States Geological Survey (USGS) estimates suggest that North Slope shale plays, including the Shublik Formation, have huge potential for oil and gas production (Houseknecht et al., 2012a). This thesis presents a simulation study of oil production from a typical shale oil well using data from the Eagle Ford Shale, analogous to the Shublik Formation, in order to:

- Identify significant matrix and hydraulic fracture parameters affecting production performance in shale reservoirs
- Predict expected production behavior from a typical well in ductile shale reservoirs such as the Eagle Ford (and by analogy, the Shublik Shale)
- Present a workflow for proper modeling of hydraulic fractures in the simulation of shale wells

## Chapter 2 Literature Review

### 2.1 U.S. Shale Plays

The first large-scale shale gas production in the U.S. began in the 1980s and 1990s when Mitchell Energy and Development Corporation started production from the Barnett Shale in North-Central Texas. By the end of 2005, the Barnett Shale alone was producing 0.5 trillion cubic feet of natural gas per year (Energy Information Administration (EIA) U.S. shale report, 2011).

The success of the Barnett Shale and its geologic equivalent, the Fayetteville Shale in Arkansas, resulted in the development of other shale plays including the Marcellus, Bakken, Haynesville, Woodford, and Eagle Ford. Figure 3 shows a map of U.S. shale plays in the lower forty-eight states (EIA U.S. shale report, 2011).

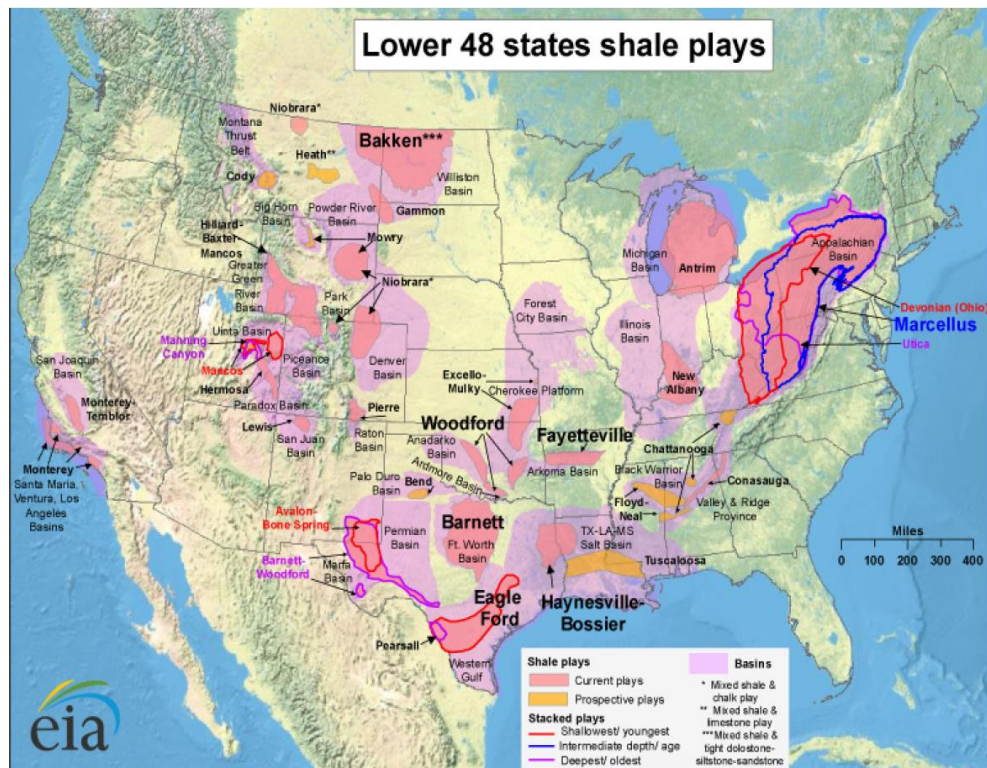


Figure 3: U.S. shale gas and shale oil plays (EIA U.S. shale report, 2011).

According to the EIA U.S. shale report (2011), development of new shale plays has increased dry shale gas production in the United States from 1.0 trillion cubic feet in 2006 to 4.8 trillion cubic feet in 2010, or 23% of total U.S. dry natural gas production. Wet shale gas reserves increased to about 60.64 trillion cubic feet by the end of 2009, when they comprised about 21% of overall U.S. natural gas reserves, and are now at the highest level since 1971 (EIA U.S. shale report, 2011). Oil production from shale plays has also grown in recent years, particularly in the Bakken Shale of North Dakota and Montana and in the Eagle Ford Shale of central Texas.

It must be noted that there is a huge difference between oil shale and shale oil reservoirs. Oil shale is a rock that contains a solid organic compound known as kerogen that must be heated in a special process, known as retorting, to generate liquid hydrocarbons. However, shale oil does not have to be heated in a well, and the oil produced directly from it is premium crude (Chaudhary, 2011).

Table 1 presents the INTEK, Inc. shale resources report for the discovered but undeveloped portions of 20 shale plays in the lower forty-eight states. INTEK estimates for technically recoverable natural gas and oil are 750 trillion cubic feet of gas and 23.9 billion barrels of oil (EIA U.S. shale report, 2011).

Eighty-six percent of recoverable shale gas resources are located in the Northeast, Gulf Coast, and Southwest regions. The largest shale gas plays are the Marcellus (410.3 trillion cubic feet or 55% of the total), Haynesville (74.7 trillion cubic feet or 10% of the total), and Barnett (43.4 trillion cubic feet or 6% of the total). The largest shale oil plays are the Monterey/Santos, Bakken, and Eagle Ford shale plays, with approximately 15.4, 3.6, and 3.4 billion barrels of technically recoverable oil, respectively (EIA U.S. shale report, 2011).

Table 1: INTEK estimates of undeveloped technically recoverable shale gas and shale oil resources remaining in discovered shale plays as of January 1, 2009 (EIA U.S. shale report, 2011).

Onshore Lower-48 Oil and Gas Supply Submodule region	Shale Play	Shale Gas Resources (Trillion Cubic Feet)	Shale Oil Resources (Billion Barrels)
<b>Northeast</b>	Marcellus	410	--
	Antrim	20	--
	Devonian Low Thermal Maturity	14	
	New Albany	11	--
	Greater Siltstone	8	--
	Big Sandy	7	--
	Cincinnati Arch	1	--
	Subtotal	472	--
	Percent of total	63%	--
	<b>Gulf Coast</b>	Haynesville	75
Eagle Ford		21	3
Floyd-Neal & Conasauga		4	--
Subtotal		100	3
Percent of total		13%	14%
<b>Mid-Continent</b>	Fayetteville	32	--
	Woodford	22	--
	Cana Woodford	6	--
	Subtotal	60	--
	Percent of total	8%	--
<b>Southwest</b>	Barnett	43	--
	Barnett-Woodford	32	--
	Avalon & Bone Springs	--	2
	Subtotal	76	2
Percent of total	10%	7%	
<b>Rocky Mountain</b>	Mancos	21	--
	Lewis	12	--
	Williston-Shallow Niobraran	7	--
	Hilliard-Baxter-Mancos	4	--
	Bakken	--	4
	Subtotal	43	4
Percent of total	6%	15%	
<b>West Coast</b>	Monterey/Santos	--	15
	Subtotal	--	15
Percent of total	--	64%	
Total onshore Lower-48 States		750	24

## **2.2 Description of Shublik Formation**

The Shublik Formation is a lithologically heterogeneous Triassic interval that is a major source rock for hydrocarbon accumulations on the North Slope. In the subsurface at Prudhoe Bay, the Shublik Formation is relatively thin (0-585 ft thick) and is underlain by the Eileen Sandstone and overlain by the Sag River Sandstone (Figure 4). All three units are truncated to the north where they overlap the Barrow Arch or have been removed by erosion. The Triassic units dip southward in the subsurface, across the North Slope to the foothills of the Brooks Range, where they, or their distally equivalent units, appear as outcrops within thrust sheets (Parrish et al., 2001; Kelly, 2004). This interval is exposed in the northeastern Brooks Range, where the Eileen Sandstone equivalent is the Fire Creek Siltstone, the Sag River equivalent is the Karen Creek Sandstone, and the intervening Shublik Formation varies from 121 to 546 ft thick (Parrish et al., 2001).

The Fire Creek Siltstone is the upper member of the Ivishak Formation at Fire Creek. The Eileen Sandstone and Fire Creek Siltstone are interpreted to be genetically related to the Shublik Formation, whereas the overlying Karen Creek and Sag River Sandstones appear to be part of a subsequent depositional sequence (Parrish et al., 2001).

The Shublik Formation is interpreted as having been deposited under the influence of oceanic upwelling, as indicated by its vertical and lateral lithologic variability and its phosphatic, organic-rich, and glauconitic composition (Figure 5; Kelly, 2004).

### **2.2.1 Subsurface Shublik Formation Stratigraphy**

During equity negotiations and establishment of picks for the Prudhoe Bay unit common database, the subsurface Shublik was subdivided into four geophysically distinct zones (Figure 4; Kupecz, 1995; Hulm, 1999). These zones are labeled D through A, from the base to the top of the section. This subdivision is still in use today.

**Zone D**

The basal unit of the Shublik Formation is massive fine- to medium-grained, noncalcareous, well-sorted, phosphatic sandstone with thicknesses of 0 to 24 ft (Hulm, 1999).

**Zone C**

This zone is composed predominantly of black shale and dark-gray lime packstone/grainstone, with the latter dominating upwards. Thicknesses range from 0 to 46 ft. The shales are very organic-rich and extremely fossiliferous (Hulm, 1999).

**Zone B**

This zone is characterized by phosphorite, phosphatic carbonate, and siliciclastic rocks; thickness varies from 0 to 28 ft (Hulm, 1999).

**Zone A**

This is the uppermost unit in the Shublik Formation and is lithologically similar to zone C. Thickness of this zone ranges from 0 to 83 ft. The base of zone A is comprised of black shale that grades upward into dark-gray grainstone and packstone (Hulm, 1999).

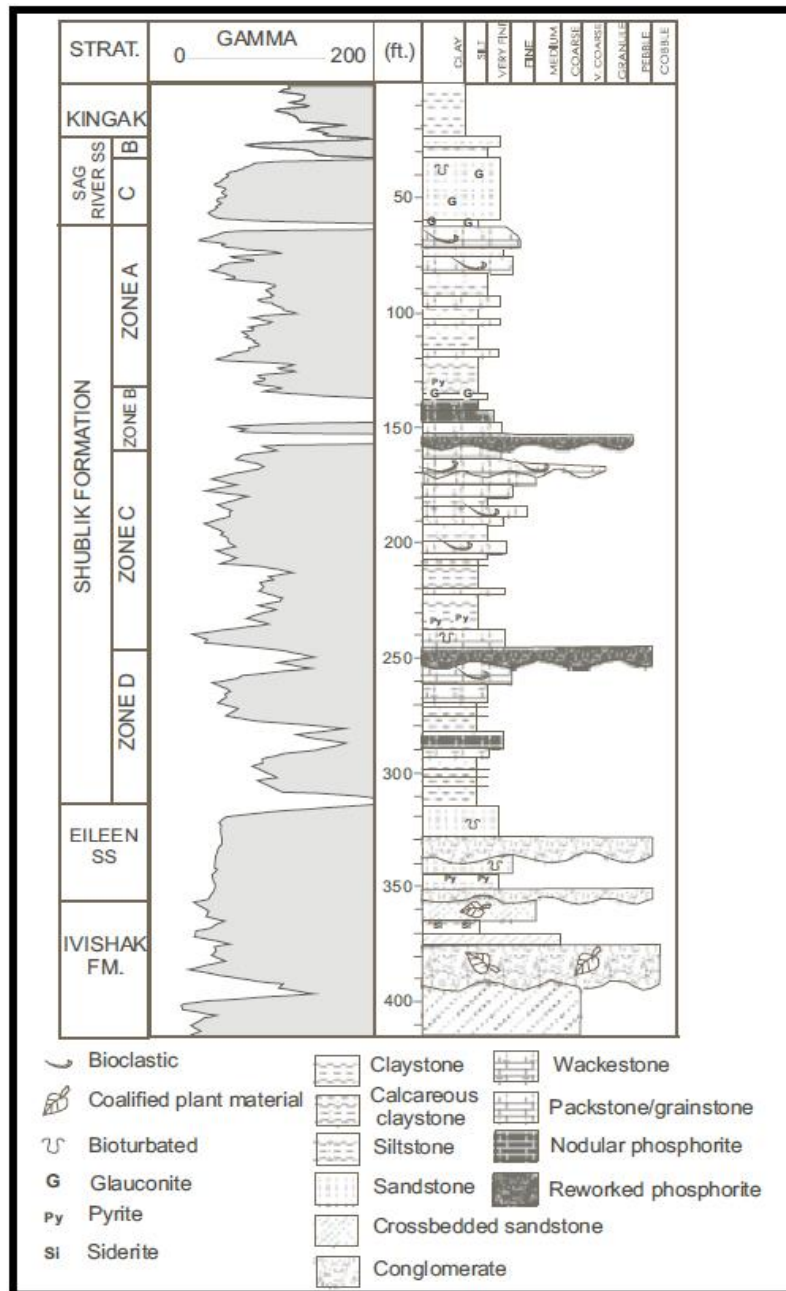


Figure 4: Typical lithostratigraphy and corresponding gamma ray log response for the Eileen Sandstone, Shublik Formation, and Sag River Sandstone based on the wells in and around Prudhoe Bay (Hulm, 1999).

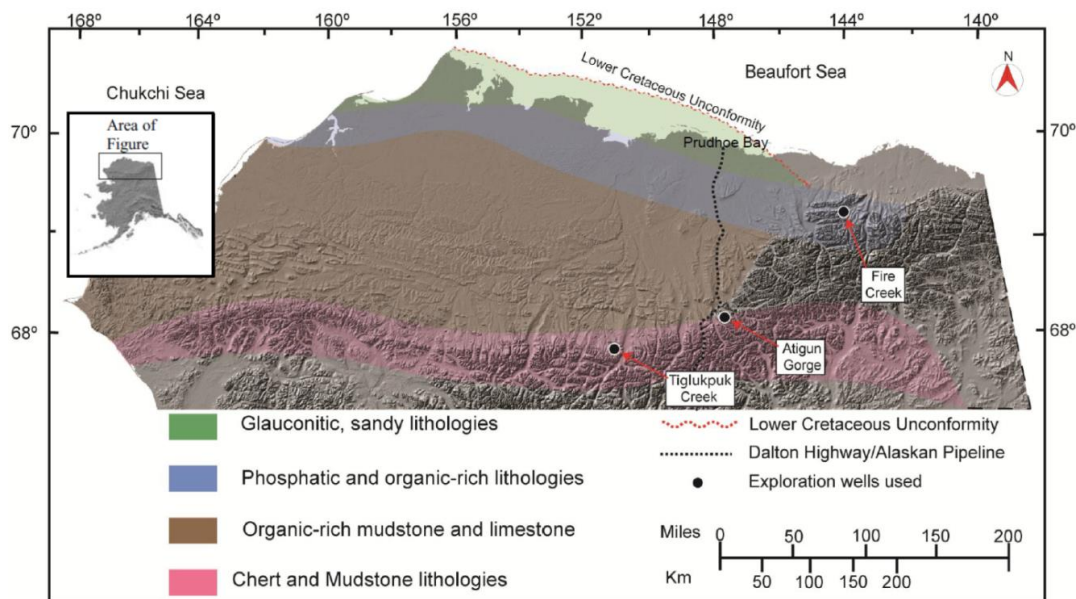


Figure 5: Map of Northern Alaska showing lithologic facies of Shublik Formation (Kelly, 2004).

## 2.2.2 Shublik Formation Potential as a Shale Resource Play

Houseknecht et al. (2012a) studied the oil and gas potential of the Shublik Formation. The Shublik Formation contains a mixture of Type I (hydrogen to carbon ratio  $> 1.25$  and oxygen to carbon ratio  $< 0.15$ ) and type IIS (hydrogen to carbon ratio  $< 1.25$ , oxygen to carbon ratio 0.03 to 0.18 and high sulfur content) kerogens. Shublik-sourced conventional oil has low gravity (23-39 °API) and high sulfur content ( $> 1.5\%$ ). The Shublik Formation rocks occur at depths ranging from less than 3,000 ft at the Barrow Arch to greater than 20,000 ft in the Brooks Range. Depth variation and subsequent variations in thermal maturity resulted in an oil window in the north and a dry gas window in the south (Figure 6). Figure 7 shows the thickness of oil- and gas-prone parts of the Shublik Formation. The Houseknecht et al. (2012b) assessment, based on Total Organic Carbon (TOC), hydrogen index (HI), and formation thickness, identified the best oil potential within the shale oil Assesment Unit (AU) and gas potential in shale gas AU across the North Slope, shown in Figure 7.



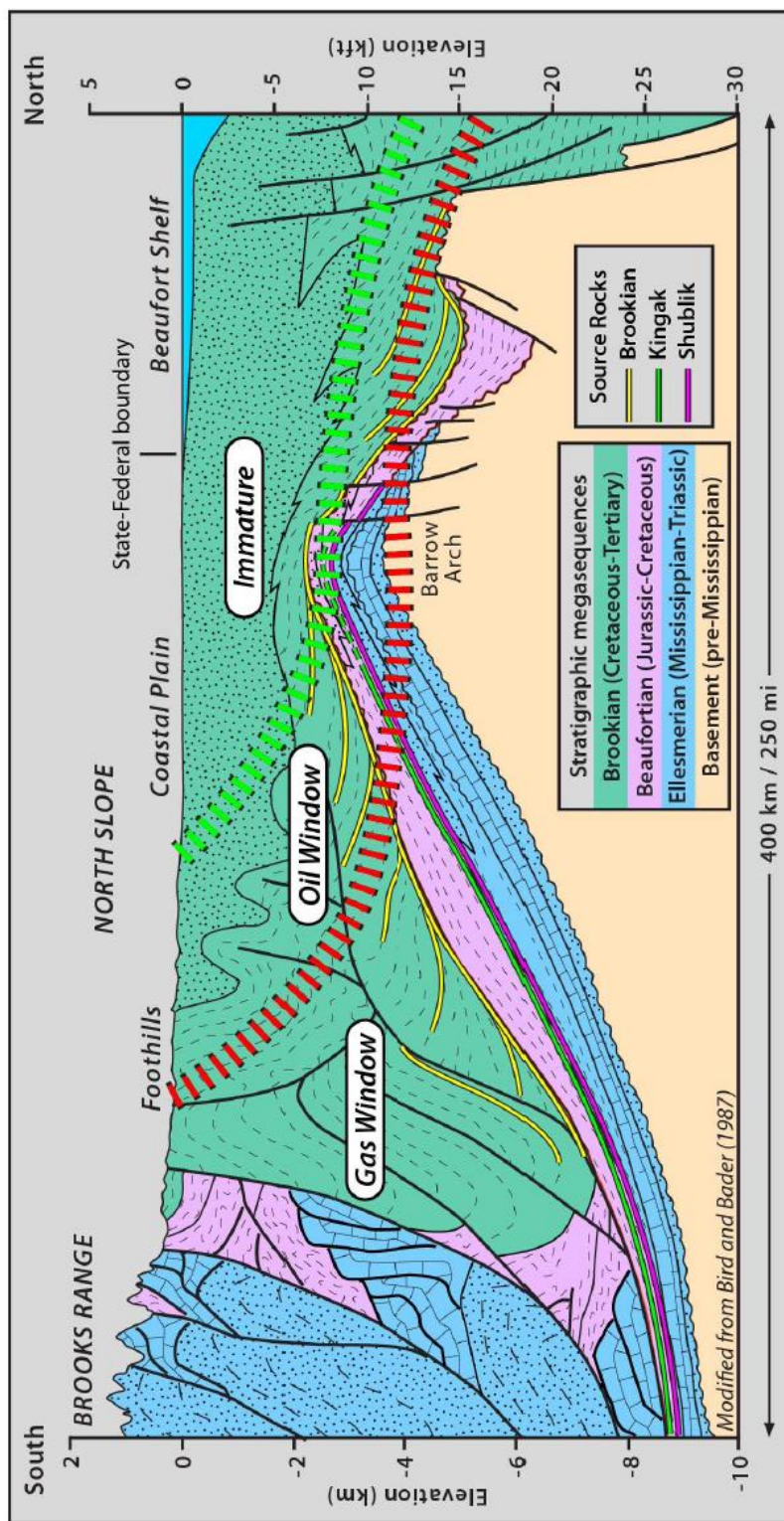


Figure 6: Generalized North-South cross section across the Central North Slope of Alaska. The stratigraphic position of Shublik is shown schematically by the pink line. Generalized thermal maturity zones are shown by the broad dashed green and red lines; source rocks are immature above the green line, are in the oil window between the green and red lines, and are in the gas window below and south of the red line (Houseknecht et al., 2012b).

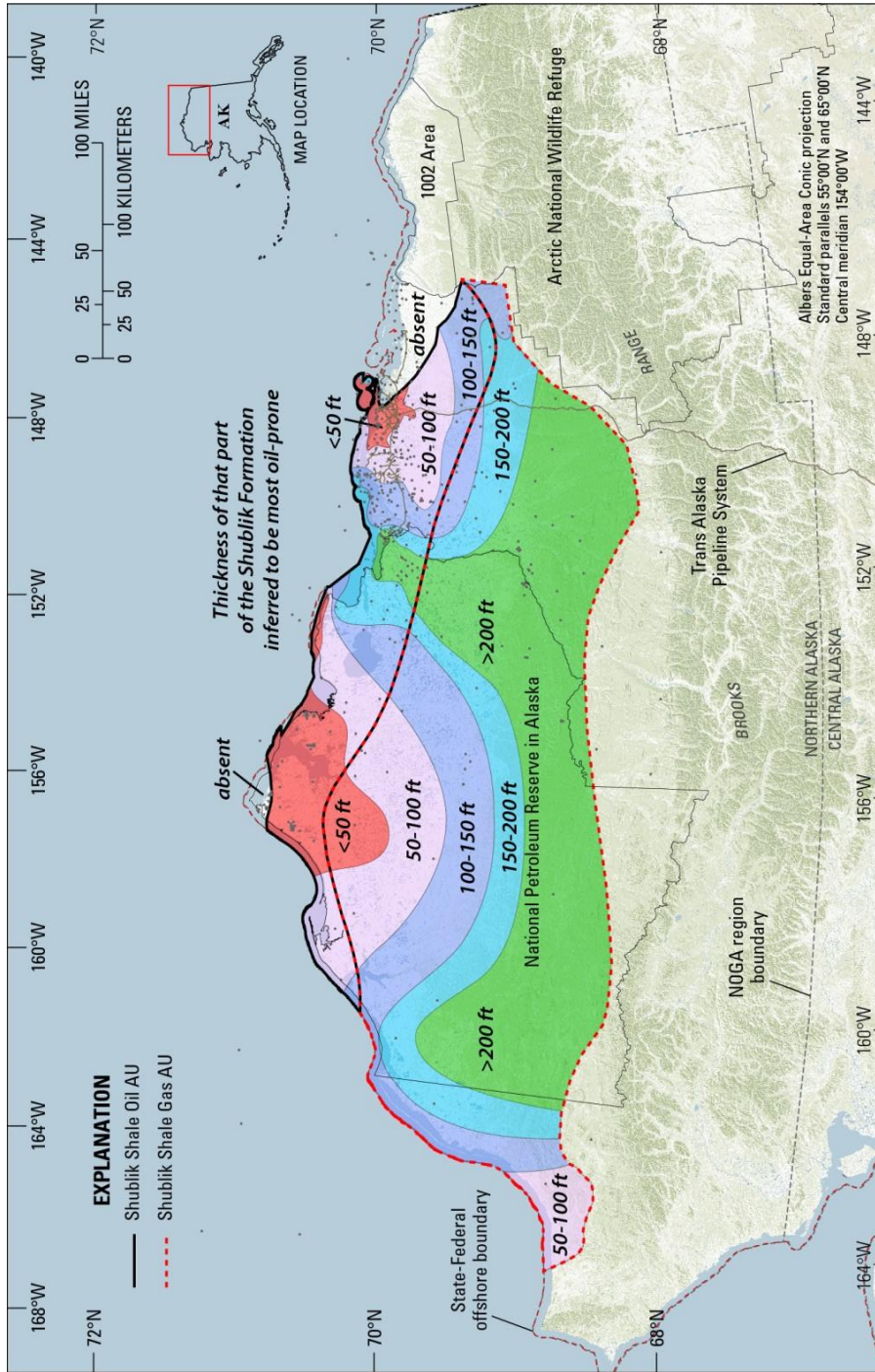


Figure 7: Map of Northern Alaska showing the thickness of oil-prone part of Shublik Formation and extent of Shublik shale oil (outlined in black) and shale gas (outlined in red dashes) (Houseknecht et al., 2012b).

The USGS Shublik Formation shale oil and shale gas assessment results are presented in Table 2. The Shublik alone has, on average, 463 MMBO (million barrels of oil) of undiscovered oil, with 462 BCFG (billion cubic feet of gas) of associated gas and 12 MMBNGL (million barrels of natural gas liquids). When combined with other potential North Slope shale resource plays, such as the Kingak shale and the Brookian shale, the USGS estimated that the North Slope of Alaska has a total potential of 940 MMBO and 42,006 BCFG of oil and natural gas (Table 3). This makes the North Slope's potential shale oil resources greater than that of the Eagle Ford Shale of Texas (Figure 8).

Table 2: USGS Shublik Formation shale oil and shale gas assessment results (Houseknecht et al., 2012a).

Assessment Units (AU)	Field Type	Total Undiscovered Resources		
		Oil (MMBO)	Gas (BCFG)	NGL (MMBNGL)
Shublik Shale Oil AU	Oil	463	462	12
Shublik Shale Gas AU	Gas	-	38,405	205

Table 3: North Slope potential compared to other U.S. shale plays (Houseknecht et al., 2012a).

<b>Shale Oil</b>	<b>USGS Estimated Undiscovered Oil (MMBO)</b>
Bakken	3,645
North Slope	940
Eagle Ford	853
Woodford	393
Niobrara	227
<b>Shale Gas</b>	<b>USGS Estimated Undiscovered Gas (BCFG)</b>
Marcellus	81,374
Haynesville	60,734
Eagle Ford	50,219
North Slope	42,006
Woodford	15,105



Figure 8: USGS estimates of undiscovered oil, showing the potential of the North Slope in comparison to major U.S. shale oil plays (Houseknecht et al., 2012a).



## 2.3 Description of the Eagle Ford Shale

### 2.3.1 Eagle Ford Shale Geology

Figure 9 shows the Eagle Ford Shale play, located in Texas. The Eagle Ford Shale trends across Texas from the Mexican Border in the south into east Texas, and is located within the Texas Maverick Basin, roughly 50 miles wide and 400 miles long. The Eagle Ford is a Late Cretaceous formation that overlies the Buda Limestone and is in turn overlain by the Austin Chalk (Figure 10). The Eagle Ford Shale has long been recognized as the source rock for conventional accumulations in the Austin Chalk (Martin et al. 2011).

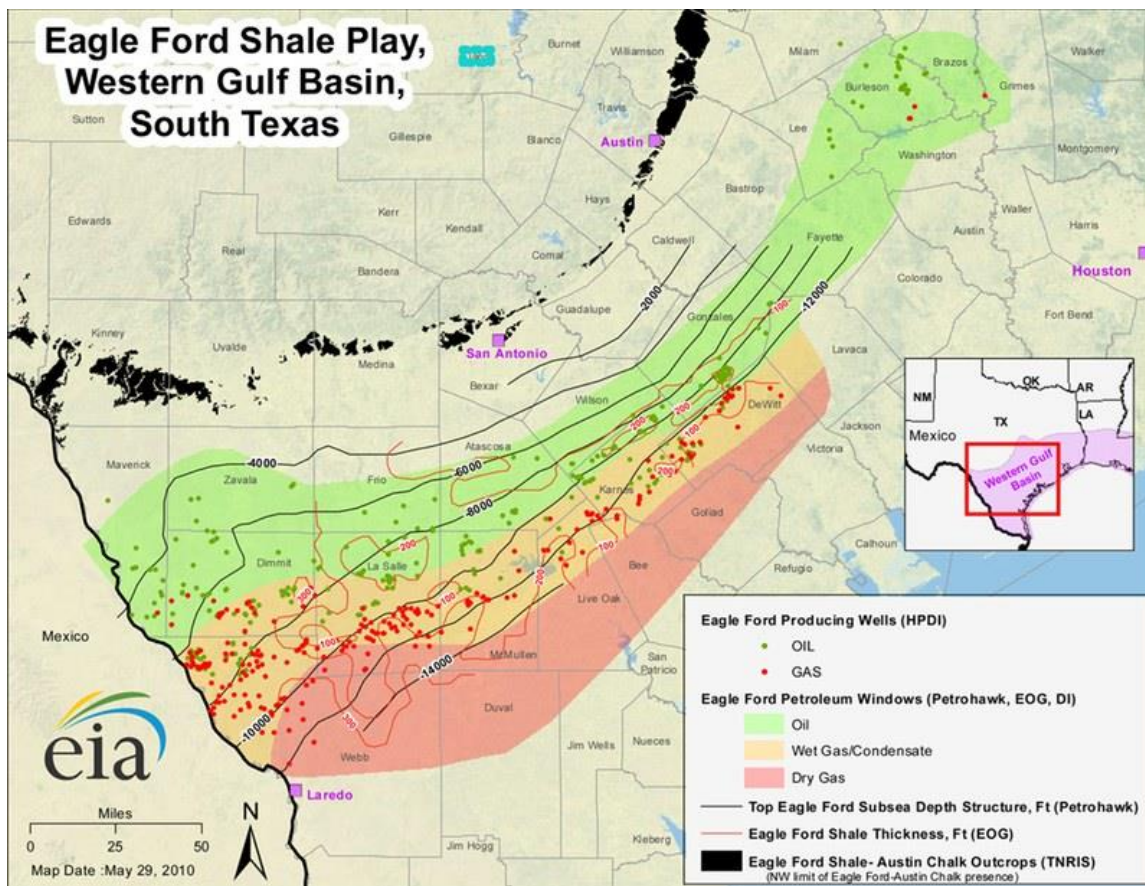


Figure 9: Eagle Ford Shale play (EIA, 2010).

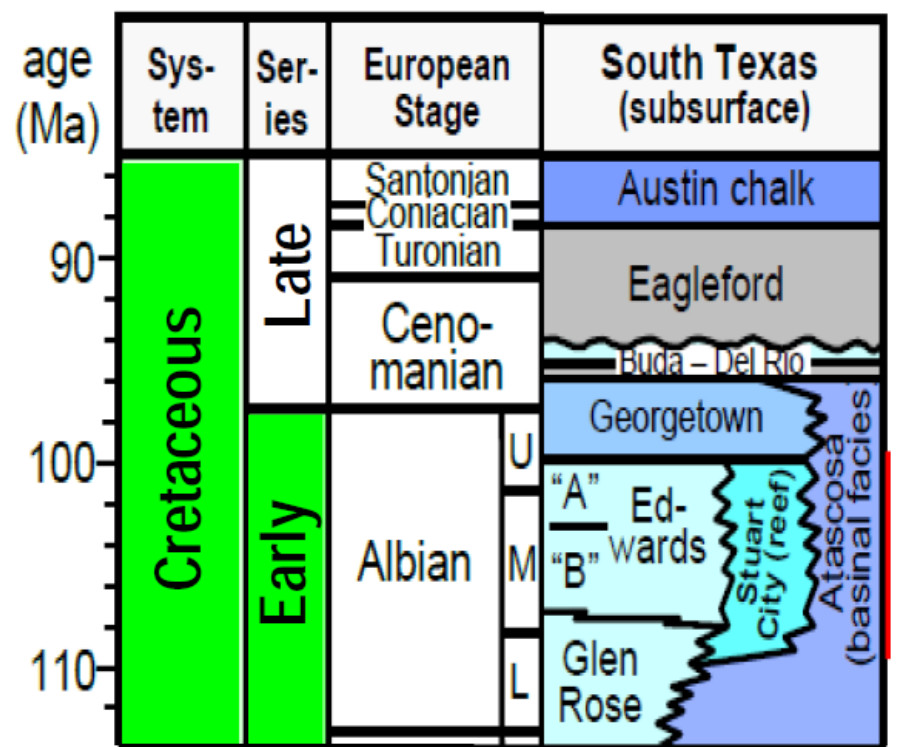


Figure 10: Upper Cretaceous stratigraphic column showing the Eagle Ford Shale (Martin et al., 2011).

The first well in the Eagle Ford Shale, located in the Hawkville field in LaSalle County, Texas, was drilled by Petrohawk in 2008. According to the Railroad Commission of Texas, there are 162 completed wells and 690 well permits in the Eagle Ford as of September 2010. According to Petrohawk Energy, the average cost ranges from 4.0 to 6.5 million dollars per horizontal well in Eagle Ford Shale (EIA U.S. shale report, 2011).

The Eagle Ford Formation's temperature is between 150 °F and 350 °F. Eagle Ford elevations range between 1,500 ft and 14,000 ft True Vertical Depth (TVD). Its thickness varies between 50 ft on the northeast side and 330 ft on the southwest side. The pay thickness is between 125 ft and 300 ft. The pressure gradient in the Eagle Ford Shale varies from 0.55 to 0.85 psi/ft (Martin et al. 2011; Chaudhary, 2011).

### 2.3.2 Eagle Ford Shale Mineralogy

Mineralogy is an important factor in deciding the economic exploitation potential of a shale reservoir and the possibility of hydraulic fracturing success. Fractures are created more easily in silica-rich and carbonate-rich shales than in clay-rich shales (Sondhi, 2011).

Sondhi (2011) identified sixteen minerals in the Eagle Ford Shale that are clustered into four groups (Table 4). Figure 11 shows the average percentage of these mineral groups present in the Eagle Ford Shale. There is an inverse linear correlation between the amount of clay and the amount of carbonates in the Eagle Ford Shale's composition. As the carbonates weight percent increases, that of clay decreases, and vice versa. This relationship is shown in detail for a typical well in Figure 12.

Table 4: Minerals identified in the Eagle Ford Shale (Sondhi, 2011).

<b>Minerals Identified</b>	
<b>Minerals</b>	<b>Groups Formed</b>
Quartz	Quartz
Calcite	Total Carbonates
Dolomite	
Siderite	
Aragonite	
Illite	Total Clays
Smectite	
Kaolinite	
Chlorite	
Mixed Clays	
Orthoclase Feldspar	Total Feldspar
Oglioclase Feldspar	
Albite	
Pyrite	Others
Anhydrite	
Apatite	

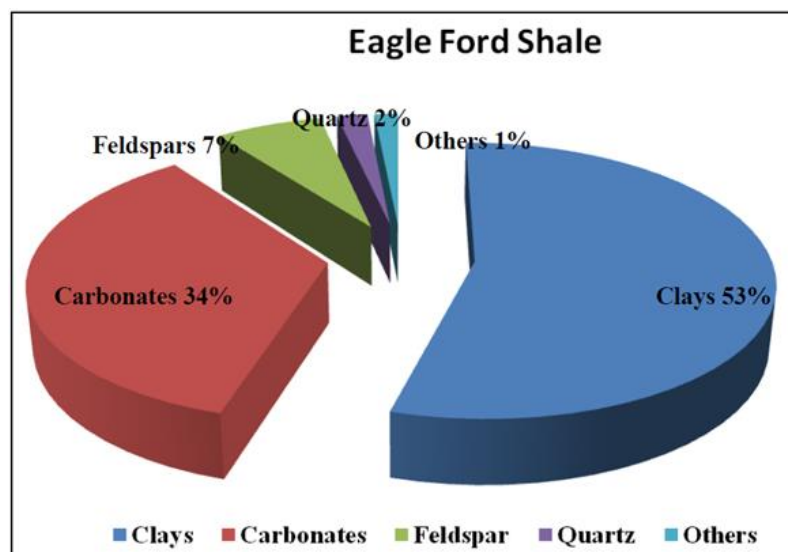


Figure 11: Eagle Ford Shale mineralogy (Sondhi, 2011).

### 2.3.3 Petrophysical Properties of the Eagle Ford

Figure 12 shows the petrophysical properties plotted against depth for a typical well in the Eagle Ford Shale oil window. Clay and carbonate show an inverse linear correlation throughout the depth of the well. Helium porosity follows the clay trend and increases as clay content increases and carbonate decreases. Total organic carbon has a linear correlation with carbonate, showing that higher TOC is observed for higher carbonate content (Sondhi, 2011). Based on these correlations, Sondhi (2011) identified two distinct petrophysical groups, Petrotype I and Petrotype II. Petrotype I is clay rich, carbonate poor, with low TOC and higher porosity. Petrotype II is carbonate rich, clay poor, and has a higher TOC and lower porosity (Sondhi, 2011). Average values for these two groups are listed in Table 5.



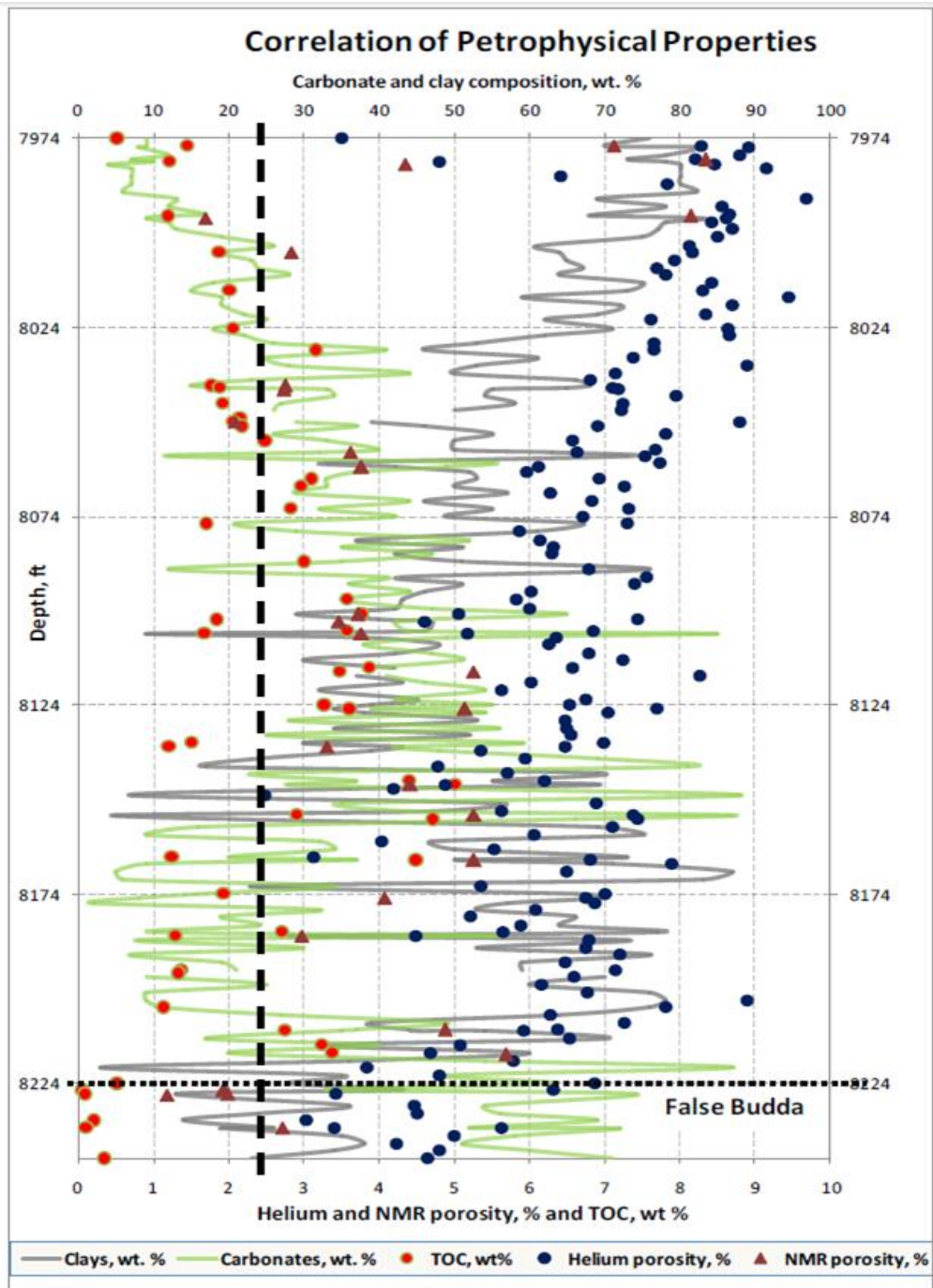


Figure 12: Eagle Ford petrophysical properties plotted against depth (Sondhi, 2011).

Table 5: Average values for petrophysical properties of two petrotypes identified in the Eagle Ford oil window (Sondhi, 2011).

<b>Petrotypes</b>	<b>Average Carbonates, %</b>	<b>Average Clays, %</b>	<b>Average Helium Porosity, %</b>	<b>Average TOC, wt%</b>
Petrotype I	14	72	8	1.81
Petrotype II	45	43	7	3.30

Due to low TOC and high clay content, Petrotype I is not a good candidate for production. However, Petrotype II, with its higher carbonate content and TOC, moderate clay, and porosity, can be a good interval for production (Sondhi, 2011).

#### **2.3.4 PVT Behavior in the Eagle Ford Shale**

The thermal maturity of the Eagle Ford varies regionally. The Eagle Ford goes through three maturation windows as it dips south and increases in depth (Martin et al. 2011). This has resulted in three different fluid zones: oil, gas condensate, and dry gas. Figure 13 shows the variation of the Eagle Ford fluid types based on the average Gas-Oil Ratio (GOR) from three months of production (Tian et al., 2013). According to Wan et al. (2013), maturity in the Eagle Ford is a function of depth. The oil window is located in the shallow north-western part of the formation, while dry gas window is located in the deeper south-eastern part. Based on the EIA U.S. shale report (2011), and Martin et al. (2011), the approximate depth of oil, condensate, and dry gas producing zones are 8,000 ft, 10,000 ft, and 14,000 ft, respectively. The areas of the dry gas, condensate, and oil zones are estimated to cover 200, 890, and 2,233 square miles, respectively.

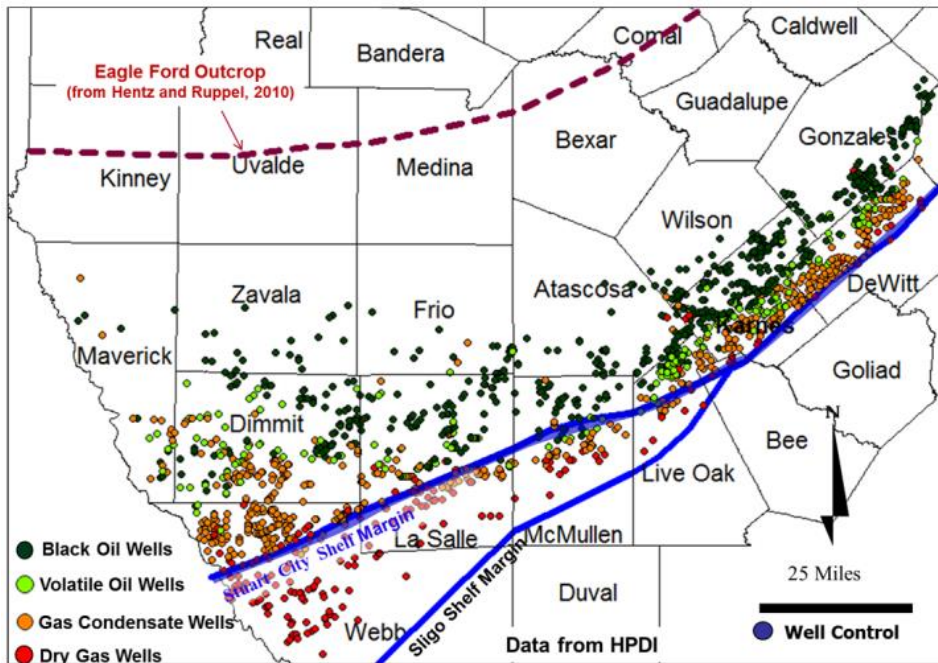


Figure 13: Fluid type variations in the Eagle Ford Shale (Tian et al., 2013).

Due to the long transient flow time in low permeability shale reservoirs, bottom hole and surface fluid samples may not be good representatives of in-situ reservoir fluid. However, the most common method for PVT analysis is still collecting produced gas and liquid samples at the surface and recombining them in a laboratory (Whitson and Sunjerga, 2012).

Orangi et al. (2011) developed a set of synthetic Eagle Ford fluids by recombining typical stock tank oil and gas compositions. Available data for their study were stock tank oil API gravity, Gas-Oil Ratio (GOR), Condensate-Gas Ratio (CGR), reservoir temperature, and reservoir pressure. Orangi et al. (2011) adjusted the recombined compositions to yield reservoir fluids with different GOR values of 500, 1000, and 2000 SCF/STB, and different CGR values of 30, 100, 150, and 200 STB/MMSCF. Tables 6 and 7 summarize recombined compositions for oil and gas-condensate fluids with different GOR/CGR values developed by Orangi et al. (2011), based on the Peng and Robinson (1976) equation of state.

Table 6: Molar composition of synthetic Eagle Ford oil (Orangi et al., 2011).

Component	Molecular Weight	Specific Gravity	T <sub>c</sub> (R)	P <sub>c</sub> (psia)	Composition (mole %)		
					GOR (SCF/STB)		
					500	1000	2000
C1	16.04	0.3500	343.3	673.1	31.23	44.52	56.45
N2	28.01	0.8080	227.2	492.3	0.07	0.10	0.13
C2	30.07	0.4800	549.8	708.4	4.31	5.88	7.29
C3	44.10	0.5077	665.8	617.4	4.15	4.51	4.83
CO2	44.01	0.8159	547.6	1071.3	1.28	1.82	2.31
IC4	58.12	0.5631	734.6	529.1	1.35	1.30	1.25
NC4	58.12	0.5844	765.4	550.7	3.38	2.98	2.62
IC5	72.15	0.6248	828.7	483.5	1.81	1.51	1.24
NC5	72.15	0.6312	845.6	489.5	2.14	1.71	1.33
NC6	86.18	0.6641	914.2	439.7	4.62	3.28	2.08
C7 - C10	114.40	0.7563	1060.5	402.8	16.30	11.56	7.32
C11 - C14	166.60	0.8135	1223.6	307.7	12.00	8.94	5.92
C15 - C19	230.10	0.8526	1368.4	241.4	10.04	7.13	4.51
C20+	409.20	0.9022	1614.2	151.1	7.31	4.76	2.75

Table 7: Molar composition of synthetic Eagle Ford gas condensates (Orangi et al., 2011).

Component	Molecular Weight	Specific Gravity	T <sub>c</sub> (R)	P <sub>c</sub> (psia)	Composition (mole %)			
					CGR (STB/MMSCF)			
					30	100	150	250
C1	16.04	0.3500	343.3	673.1	74.73	70.75	65.88	63.74
N2	28.01	0.8080	227.2	492.3	0.18	0.17	0.15	0.15
C2	30.07	0.4800	549.8	708.4	9.43	8.94	8.34	8.07
C3	44.10	0.5077	665.8	617.4	5.24	4.98	4.67	4.53
CO2	44.01	0.8159	547.6	1071.3	3.05	2.89	2.69	2.60
IC4	58.12	0.5631	734.6	529.1	1.14	1.10	1.05	1.02
NC4	58.12	0.5844	765.4	550.7	1.96	1.90	1.83	1.79
IC5	72.15	0.6248	828.7	483.5	0.79	0.81	0.83	0.83
NC5	72.15	0.6312	845.6	489.5	0.69	0.73	0.79	0.82
NC6	86.18	0.6641	914.2	439.7	0.24	0.67	1.19	1.42
C7 - C10	112.00	0.7527	1051.4	408.6	1.67	4.28	7.63	9.10
C11 - C14	175.00	0.8201	1245.9	296.9	0.81	2.56	4.55	5.43
C15 - C19	210.00	0.8424	1327.6	259.0	0.06	0.16	0.28	0.33
C20+	250.00	0.8612	1405.8	226.3	0.03	0.08	0.14	0.16

A black oil model can be used in the Eagle Ford oil window where initial reservoir pressure is well above the bubble point pressure. Using a black oil model can reduce simulation time and calculations. Table 8 summarizes the black oil PVT properties for the Eagle Ford Shale in the oil window used by Chaudhary et al. (2011).

Table 8: Black oil PVT properties for the Eagle Ford oil window (Chaudhary et al., 2011).

Reservoir temperature, °F	255
Bubble point pressure for oil, psi	2398
Solution gas oil ratio, SCF/STB	650
Oil °API gravity	42
Under-saturated oil compressibility, psi <sup>-1</sup>	1×10 <sup>-5</sup>
Gas specific gravity	0.8

### 2.3.5 The Eagle Ford Shale as a Possible Analog for the Shublik Shale

The Eagle Ford Shale has been proposed as an analog for the Shublik Formation (Hutton et al., 2012). As seen in Table 9, the Eagle Ford Shale and the Shublik shale appear to have similar TOC values and kerogen types. Thermal maturity and mechanical properties are also similar. These similarities make the Eagle Ford a possible analog for the Shublik, suggesting that the Shublik may respond to hydraulic fracture treatments similarly to the Eagle Ford. However, the Shublik may require different completion and stimulation strategies due to differences in age, lithology, in situ stress orientation, and depths (Hutton et al., 2012). Shublik oil seems to be heavier than Eagle Ford oil; therefore, depending on its GOR and in-situ viscosity, its production performance could be different.

Table 9: Similar characteristics of the Eagle Ford Shale and the Shublik shale (Hutton et al., 2012).

	<b>Eagle Ford</b>	<b>Shublik</b>
<b>Total Organic Carbon (TOC), %</b>	2 - 7	2 - 4
<b>Main Kerogen Types</b>	I/II (oil)	I/II-S (oil)
<b>Oil Gravity, °API</b>	30 - 50	24
<b>Thickness, ft</b>	50 - 250	0 - 600
<b>Thermal Maturity</b>	Immature - Oil - Gas	Immature - Oil - Gas
<b>Lithology and Variability</b>	Shale - Siltstone - Shale	Shale - Siltstone - Limestone
<b>Brittleness</b>	Yes - Quartz	Yes - Calcite
<b>Overpressure</b>	Yes	Locally

Table 10 summarizes the reservoir simulation parameters collected for the Eagle Ford Shale and available data for the Shublik Formation, modified from Decker (2012). The currently available data for the Shublik Formation is scarce; therefore, data from the Eagle Ford is used in this study.

Table 10: Reservoir simulation parameters (modified from Decker, 2012).

	<b>Eagle Ford</b>	<b>Shublik</b>
<b>Matrix Permeability, nd</b>	50 – 300 (Organic rich – calcite rich) Average used in simulation: 150–200	-
<b>Matrix Porosity, %</b>	7– 15 Average used in simulation: 5 – 6	-
<b>Depth to the Top of Formation, ft</b>	Oil Window: 8,000 Condensate zone: 10,000	-
<b>Reservoir Initial Pressure, psi</b>	Average used in simulation of oil window : 6400–6500	-
<b>Thermal Maturity, Fluid Type and PVT</b>	Oil, Gas condensate and Dry Gas window Average $P_b$ in oil window : 2400 psia	-
<b>Reservoir Thickness, ft</b>	50 – 250 Average used in simulation: 200	0 – 600
<b>Oil <sup>o</sup> API gravity</b>	30 – 50	24 - 45
<b>Initial Water Saturation, %</b>	Average used in simulation: 30	-
<b>Reservoir Temperature, °F</b>	Average used in simulation: 250	-
<b>Average Rock Compressibility, psia<sup>-1</sup></b>	Approximate value used in simulations: $5 \times 10^{-6}$	-
<b>Presence of Natural Fractures</b>	Probably, but not documented	Yes, but not documented

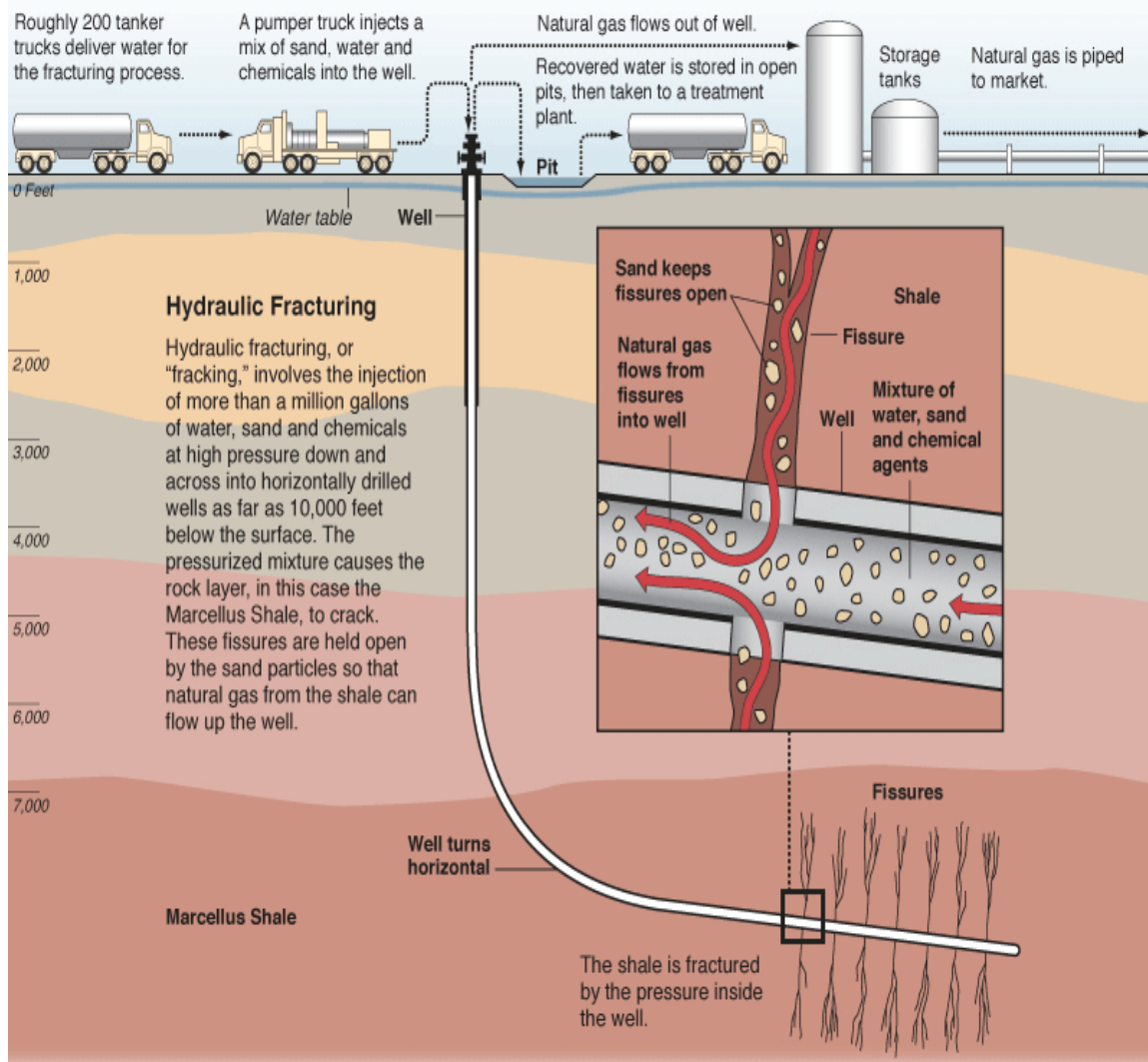


## 2.4 Hydraulic Fracturing

Shale reservoirs have very low permeability. In order to produce oil and gas at economic flow rates, flow paths must be created. Horizontal drilling coupled with hydraulic fracturing has proven to be an effective solution. Hydraulic fracturing is a method of enhancing oil and gas recovery from wells by injecting water, sand, and chemicals into rock formations under very high pressure to fracture the rock and create flow paths for stored hydrocarbons (Suchy and Newell, 2011).

Figure 14 is a graphical description of the multi-stage hydraulic fracturing process in a horizontal well. For each well, depending on the number of stages and properties of formation, large volumes of fracturing fluid (mainly water) are injected at rates greater than what the formation can take. In a typical well stimulation, the total volume is on the order of a few million gallons. Injection at rates higher than intake causes the pressure to build up and eventually fractures the formation perpendicular to the minimum local stress. To ensure that fracture remains open after pumping stops, solid particles called proppant are injected into the fracture (Nolen, 2013).

Figure 15 represents fluid flow in hydraulically fractured shale reservoirs. In the absence of natural fractures in the matrix, fluid flows from the matrix into the hydraulic fractures, then from the hydraulic fractures into the wellbore (Figure 15 (a)). If natural fractures are present in the matrix and the permeability of the hydraulic fractures is higher than that of the natural fractures (which is usually the case), fluid flows from the matrix into the natural fractures and then into the hydraulic fractures before entering the wellbore (Figure 15 (b); Tivayanonda, 2012).



Graphic by Al Granberg

Figure 14: Description of the hydraulic fracturing process ([www.propublica.org/special/hydraulic-fracturing-national](http://www.propublica.org/special/hydraulic-fracturing-national)).

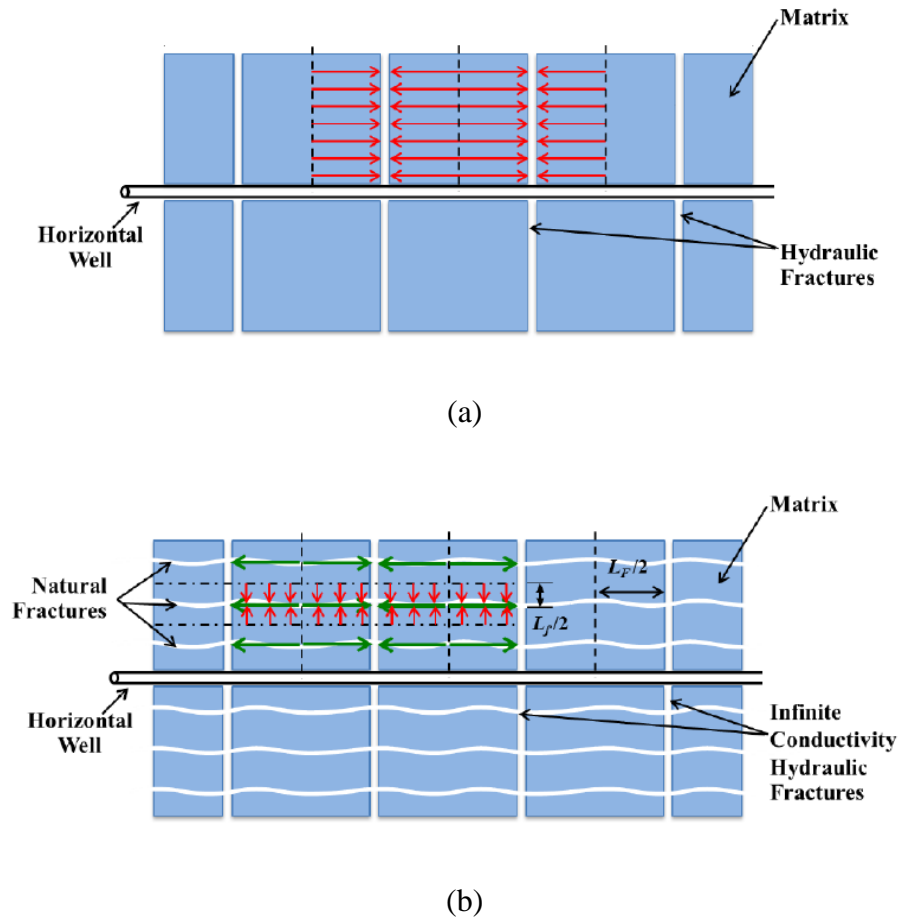


Figure 15: (a) Horizontal well with high conductivity hydraulic fractures. (b) Horizontal well with hydraulic fractures in a naturally fractured formation (Tivayanonda, 2012).

### 2.4.1 Propped Zone and Unpropped Zone

As proposed by Warpinski (2009) and Cipolla et al. (2009), total fracture height can be divided into three zones depending on proppant distribution: propped zone, arch zone, and unpropped zone. As is shown in Figure 16, the bottom part of the hydraulic fracture, filled with proppant, remains relatively wide after pressure release; however, the unpropped top section is unsupported after pumping stops and tends to close after pressure release. Therefore, the propped zone has a higher conductivity compared to the

unpropped zone. Width differences between the top and bottom sections result in an almost open zone with very high conductivity, called the arch zone (Cipolla et al., 2009). Proper modeling of this conductivity variation and its response to the closing stress is extremely important for fluid flow modeling.

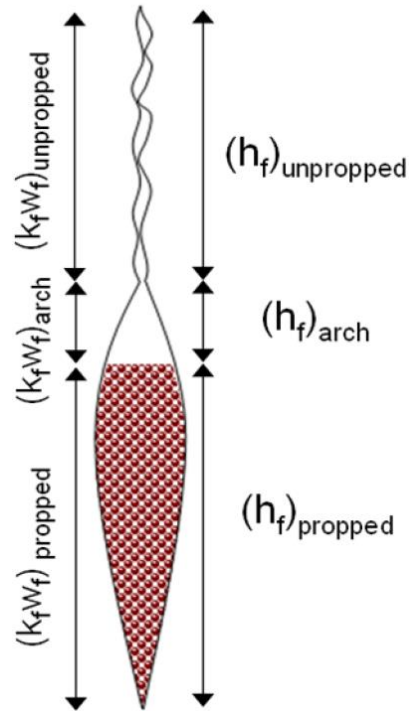


Figure 16: Vertical proppant distribution in a hydraulic fracture (Cipolla et al., 2009).

#### 2.4.2 Environmental Concerns of Hydraulic Fracturing and Wastewater Production

During hydraulic fracturing, large volumes of fracturing fluid (which is almost 99% water, as well as propping agents and chemical additives) are pumped into formations at high pressures. The goal is to create fractures in the rock and keep them open to provide flow paths for oil and gas production.

The required volume of water for hydraulic fracturing depends on the operation site and formation type. Water used in the fracturing fluid can be acquired from surface water or ground water (Environmental Protection Agency (EPA), 2010). In some locations, such as Alaska, there is limited access to surface water or shallow aquifers during a specific season. Therefore, one important issue in hydraulic fracturing is the availability of water resources.

After fracture treatment and during production, particularly in the first few months, a well can produce a large volume of water, called wastewater. Wastewater is mainly recovered fracturing fluid called ‘flowback’ that might contain chemicals and pollutants in concentrations exceeding those considered safe for drinking water. Depending on the characteristics of the fractured formation, 15% to 80% of injected fracturing fluids are recovered at the well head (EPA Research Study, 2010). Wastewater also consists of naturally occurring salts, metals, and potentially radioactive material leached from underground (Jackson et al., 2011). Therefore, proper disposal of wastewater is of fundamental importance in hydraulic fracturing and hydrocarbon extraction from shale resources.

Two other important environmental concerns in hydraulic fracturing are the contamination of drinking water resources by fracturing fluid during treatment and the migration or leakage of methane (in shale gas extraction) and wastewater to shallow water aquifers during production (Jackson et al., 2011). Osborn et al. (2011) investigated the contamination of drinking water by methane in areas of high shale gas extraction activity. Their research was performed at sites above the Marcellus and Utica formations in Pennsylvania and New York. By analyzing 60 private water wells in that region, they found methane concentrations, on average, 17 times higher in regions with drilling and production activity than in inactive areas. However, they found no evidence of contamination by fracturing fluids and wastewater (Osborn et al., 2011). Contamination of water resources by methane leakage will be less severe in shale oil wells due to the type of fluid being produced.

There are several ways to dispose wastewater in the hydraulic fracturing process. Underground injection using a permitted underground injection well is the primary disposal option. In regions such as the Marcellus Shale, where underground injection is impossible, operators may be able to send wastewater to out-of-state injection wells (Hydraulic fracturing information sheet 4, 2011). Wastewater can also be used in other hydraulic fracturing treatments. One company reported reuse of 6% of the water required for a fracturing job (Hydraulic fracturing information sheet 4, 2011). After treatment, wastewater can be discharged to surface waters (EPA Research Study, 2010). Another option is to use wastewater on dirt roads for dust suppression, particularly in areas with dust-generating surface coal mining operations (Chesapeake Energy, 2012).

Based on the above discussions, it is important to have a good estimate of recovered fracturing fluid, as well as its production rate and production time, to investigate and implement disposal options.

## 2.5 Modeling of Shale Reservoirs

Proper modeling of multistage hydraulic fractures and complex natural fracture networks, as well as their interaction with each other and with the shale matrix, is the main challenge in reservoir modeling of shale resources. Mohaghegh (2013) classified modeling of hydraulic fractures in reservoir simulation into two approaches: Explicit Hydraulic Fracture (EHF) modeling and Stimulated Reservoir Volume (SRV). EHF modeling consists of modeling each stage of hydraulic fracturing using independent hydraulic fracture simulation software applications, developing a geological model, incorporating the modeled hydraulic fracture characteristics into the geological model, upscaling the reservoir model into a simulation model, and then executing the model to forecast the production profile of a shale reservoir. This process is tedious and time-consuming. In the easier SRV approach, after developing the geological model, a three-dimensional volume around the wellbore, with higher permeability than matrix permeability is modeled to account for the hydraulic fracture stages (Mohaghegh, 2013).

While the actual width of hydraulic fractures can be as small as 0.001 ft, Rubin (2010) showed that modeling hydraulic fractures with cells equal to their true width (around 0.001 ft) is not efficient. He proposed modification of fracture representation in the simulation model in order to run the simulation more efficiently and decrease the computation time. The representation of the hydraulic fracture in the model can be modified in several ways. As illustrated in Figure 17 (Alkough et al., 2012), one way is to scale actual fracture width ( $W_f$ ; usually 0.001 ft) to a pseudo fracture width ( $W_{pf}$ ). Since the conductivity and pore volume of the modified fracture should be the same as those of the actual fracture, the lower values of fracture permeability ( $K_f$ ) and fracture porosity ( $\phi_f$ ) are used for the modified fracture.

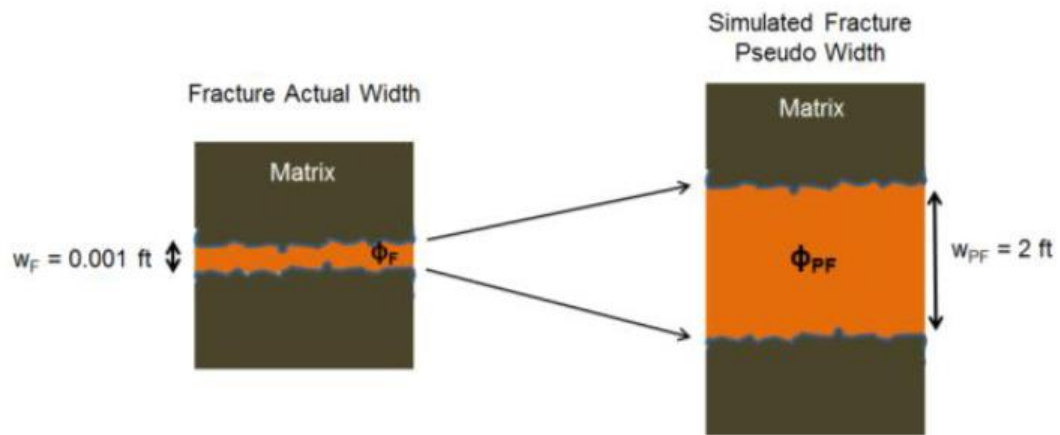


Figure 17: Modification of hydraulic fracture with porosity modifier (Alkough et al., 2012).

A simple approach for modeling hydraulic fracture geometry in reservoir simulation studies is to assume a constant fracture length over the entire height of a hydraulic fracture, while also using a constant conductivity for all simulation grid cells representing the hydraulic fracture. However, in reality, fracture dimensions and conductivity vary greatly both horizontally and vertically in the fracture plane with distance from the wellbore. Permeability/conductivity depends on the local proppant placement and concentration. As illustrated by Warpinski (2009) and Cipolla et al.(2009), the fracture height can be divided into separate zones depending on proppant distribution: a propped zone and an unpropped zone. The part of the hydraulic fracture filled with proppant remains relatively wide after hydraulic pressure release; however, the unpropped top section is left unsupported against closing stress. Therefore, this unpropped zone starts to close when the net stress increases (especially during production) and has a much lower conductivity compared to the propped zone.



## **2.6 Description of Simulators**

In this study Fracpro, a simulator developed by CARBO, was used for hydraulic fracturing design as well as for generating hydraulic fracture geometry, dimensions, propagation stages, and conductivity profiles.

CMG-IMEX, a three-phase black-oil reservoir simulator, and CMG-GEM, a three-phase compositional reservoir simulator, developed by Computer Modeling Group (CMG), were used for flow simulation and predicting production behavior. As mentioned earlier, simulation data from the Eagle Ford oil window were used for this study. In order to select the proper simulator, simulation runs were performed for a model in both CMG-IMEX and CMG-GEM modules. Results were almost the same; however, computation time was much lower for the CMG-IMEX simulator. Therefore, CMG-IMEX was selected as efficient simulator in this study.

Other CMG modules such as WinProp and Builder were used for pre-processing, while results were post-processed via Results Graph.

### Chapter 3 Methodology and Model Construction

The simulation model should include the probable completion strategy. The most common completion approach for low permeability shale reservoirs is horizontal wells with multistage hydraulic fracturing. The high conductivity hydraulic fractures form a complex matrix-fracture network, particularly in the presence of natural fractures. This hydraulically fractured zone is called the Stimulated Reservoir Volume (SRV). Figure 18 is a 2-D schematic of a typical multistage hydraulically fractured horizontal well in a shale reservoir, where the horizontal well is shown with a black line and hydraulic fractures are represented by green lines. The region inside the yellow dashed line represents the SRV. The distance between two neighboring hydraulic fracture stages is called fracture spacing.

As shown by Chaudhary et al. (2011), and Zhang and Fassihi (2013), the simulation time can be reduced significantly by assuming identical hydraulic fractures in the SRV and modeling a single fracture. The total oil production rate for a horizontal well can then be calculated by multiplying the simulation result for a single fracture by the total number of the hydraulic fractures in the stimulated volume (Chaudhary et. al, 2011). Equal length/contribution of the hydraulic fractures in SRV to fluid flow is not necessarily the case, as was addressed by Friedrich and Milliken (2013), but can be safely used to study the effect of a specific parameter or approach on simulation results.

The single hydraulic fracture chosen for reservoir simulation in this thesis is shown by the dashed blue region in Figure 18.

### 3.1 Hydraulic Fracture Design

The first step of workflow developed in this study is to model a single hydraulic fracture and generate its geometry, dimensions, propagation stages, and conductivity profile using the fracturing design software, Fracpro. Typical mechanical properties of the Eagle Ford Shale oil window, and a formation thickness of 200 ft, were used in the model (Table 11).

The job of creating one single fracture was broken down into 9 propagation stages based on the type and rate of fluid injected and the proppant concentration. The pumping schedule for the 9 propagation stages used in fracturing design is listed in Table 12. Figure 19 shows the fracture propagation stages and conductivity profile during 9 stages of pumping for one wing of the hydraulic fracture. Fracpro assumes both wings of a hydraulic fracture are equivalent and generates a profile for only one wing.

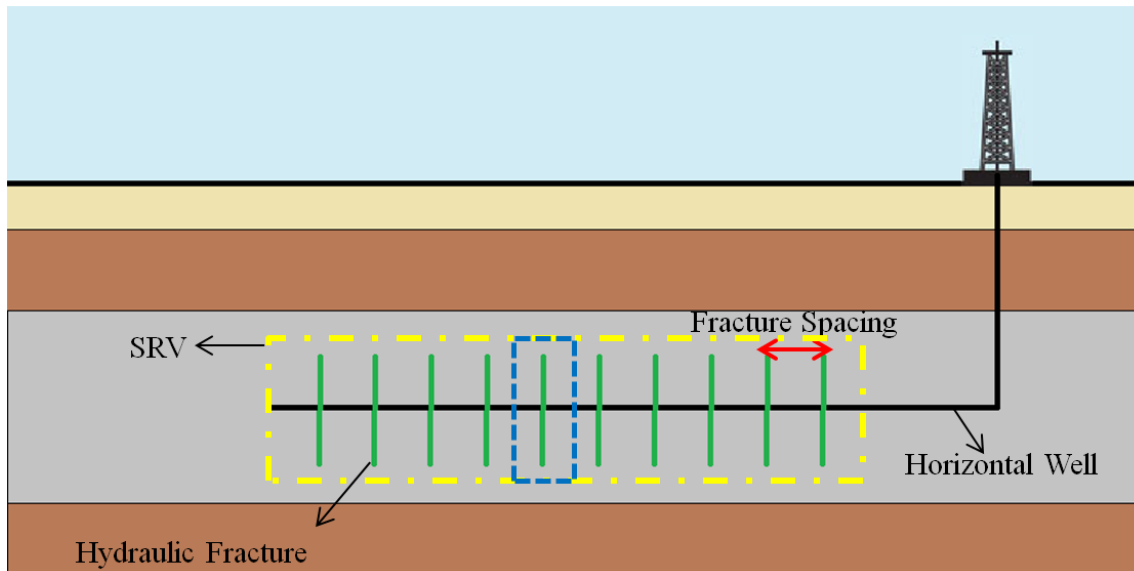


Figure 18: 2-D schematic of a multistage hydraulically fractured horizontal well in a shale reservoir. The zone separated with blue dashed lines is chosen for reservoir simulation.

Table 11: Summary of mechanical properties used for fracturing design simulation (Manchanda et al., 2012).

<b>Property</b>	<b>Value</b>
Closure Stress Gradient, psi/ft	0.7
Young's Modulus, psi	1,500,000
Poisson's Ratio	0.26
Fracture Toughness, psi.in <sup>1/2</sup>	800
Rock Embedment Strength, psi	40,000

Table 12: The typical slickwater pumping schedule of hydraulic fracturing.

Stage Number	Stage Type	Flow Rate (bpm)	Proppant Concentration (ppg)	Clean Volume (gal)	Stage Time (min)	Cumulative Time (min)	Fluid Type	Proppant Type
1	Main frac pad	45	0	1,000	0.53	0:31	Slickwater	
2	Main frac slurry	45	0.25	2,000	1.07	1:35	Slickwater	CarboProp 20/40
3	Main frac slurry	45	0.5	2,000	1.08	2:40	Slickwater	CarboProp 20/40
4	Main frac slurry	45	0.75	6,000	3.26	5:55	Slickwater	CarboProp 20/40
5	Main frac slurry	45	1	6,000	3.29	9:13	Slickwater	CarboProp 20/40
6	Main frac slurry	45	1.25	6,000	3.32	12:32	Slickwater	CarboProp 20/40
7	Main frac slurry	45	1.5	6,000	3.34	15:52	Slickwater	CarboProp 20/40
8	Main frac slurry	45	1.75	8,000	4.5	20:22	Slickwater	CarboProp 20/40
9	Main frac flush	45	0	10,000	5.29	25:40	Slickwater	

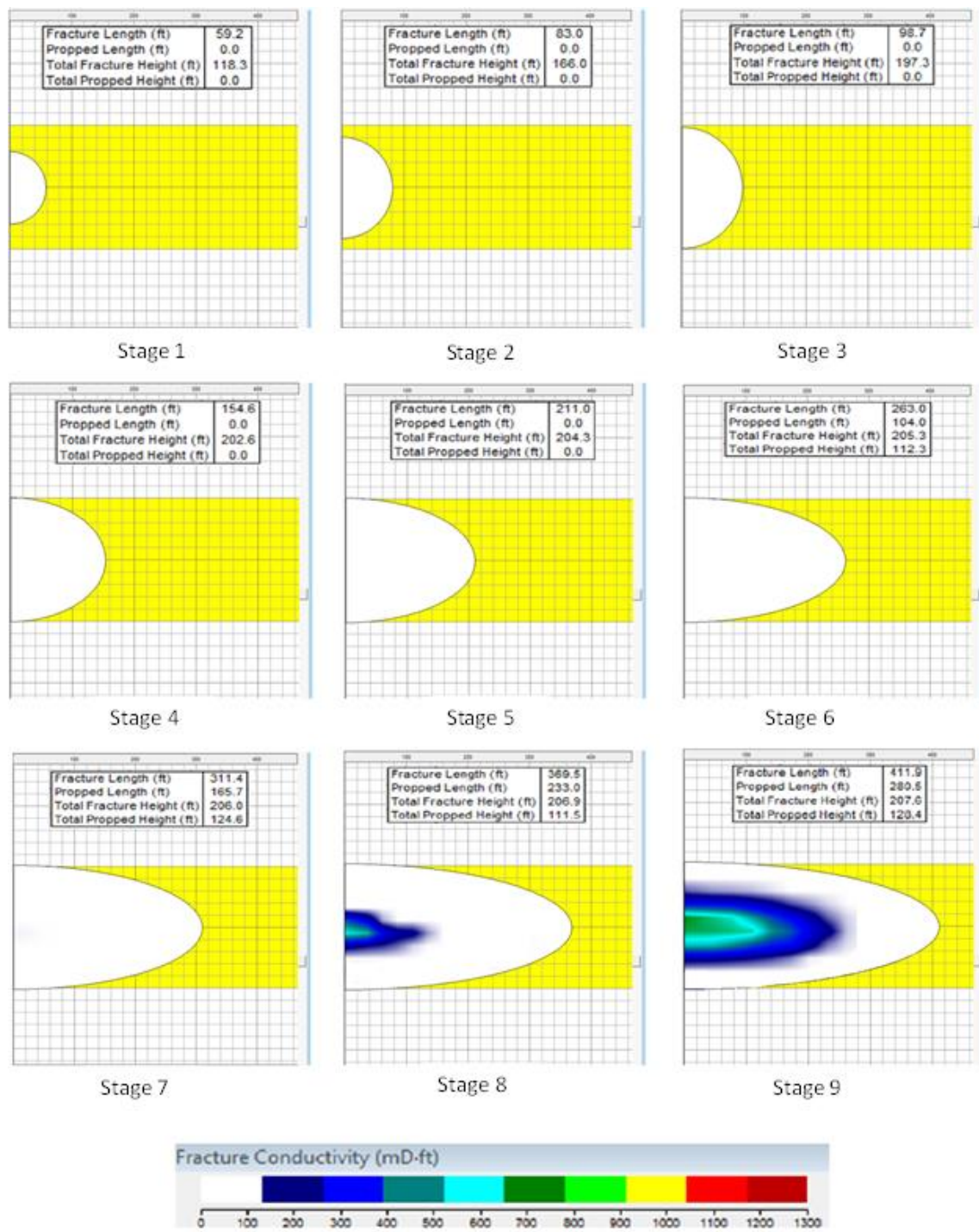


Figure 19: Fracture propagation stages generated by Fracpro.

### 3.2 Model I Description

Figure 20 (a) and (b) show a 2-D top view and 3-D view of a single hydraulic fracture model built in the CMG-Builder simulation software based on the hydraulic fracture geometry generated by Fracpro. Horizontal well blocks and hydraulic fracture blocks are shown by red and green colors, respectively. The simulation model is divided into  $31 \times 33 \times 10$  (i\*j\*k) grid blocks, for a total of 10,230. Near the hydraulic fracture, the fracture tips, and the wellbore, logarithmically spaced refined grid blocks are used to increase simulation efficiency and capture high pressure and saturation changes accurately. The natural fractures are assumed to have low density with insignificant contribution to fluid flow and therefore are excluded from the model.

The simulation model volume is determined mainly by the hydraulic fracture dimensions generated by Fracpro software, extended beyond the fracture tips into the matrix in order to capture the fluid flow and pressure depletion there. Therefore, the length of the model is the sum of the hydraulic fracture length (double of fracture half length,  $2X_f$ ) plus the distance from the tip of the fracture on both wings. Based on fracture dimensions generated in Fracpro, the fracture half-length is 412 ft, plus an additional 206 ft beyond the tips of the fracture into the matrix, making the total length of the model 1,236 ft. The width of the model is the same as the fracture spacing ( $L_f$ ), which is set at 200 ft in this model. Model thickness is equal to the formation thickness of 200 ft (Figure 20). Fracture cells are modeled with 1 ft wide blocks as suggested by the CMG software manual. Hydraulic fracture conductivity is equal to fracture permeability ( $K_f$ ) multiplied by fracture width ( $W_f$ ). Therefore, assuming a hydraulic fracture width of 1 ft makes conductivity and permeability identical. Hydraulic fracture conductivity and permeability are used interchangeably in this thesis.

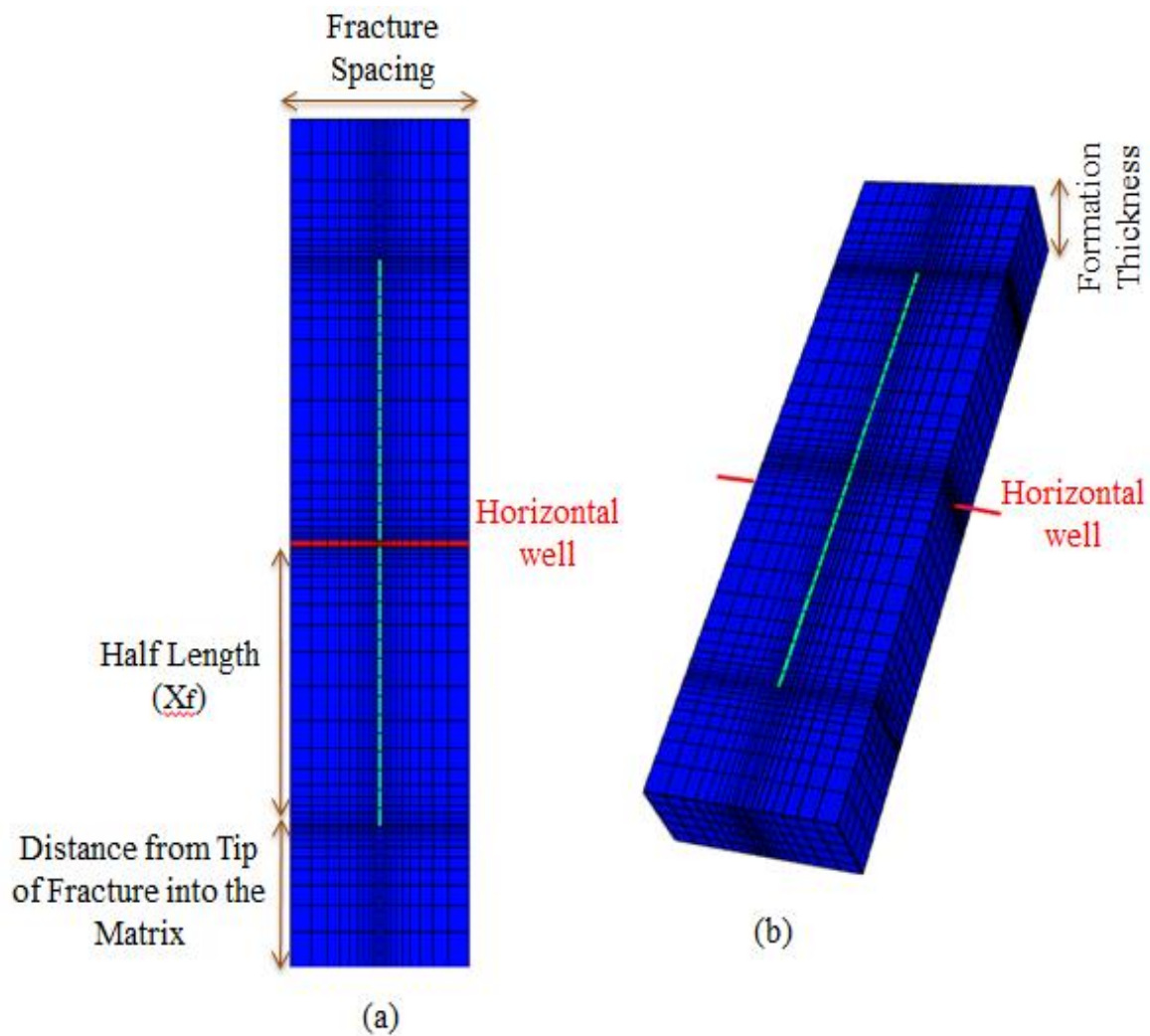


Figure 20: (a) 2-D top view of middle layer in single hydraulic fracture model. (b) 3-D view of single hydraulic fracture model.



A simple and common approach for modeling hydraulic fracture geometry in reservoir simulation studies is to assume a constant conductivity for all cells representing the hydraulic fracture. The average conductivity of a hydraulic fracture after treatment, generated by Fracpro (Figure 19 - stage 9), was 106 md.ft. Figure 21 is the side view of a single hydraulic fracture model at the fracture plane. A constant permeability of 106 md was used for all the fracture cells in Model I. The wellbore and perforation are located in the middle layer and equidistant from the boundaries. Model I ignores the presence of fracturing fluid in a hydraulic fracture and its surrounding matrix prior to production.



Figure 21: Side view of simulation model at fracture plane; matrix blocks and hydraulic fracture blocks are represented by blue and green colors, respectively.

### 3.2.1 Simulation Parameters

Model I reservoir simulation parameters are mainly based on the Eagle Ford oil window, a close analog for the Shublik Formation, collected from different sources (Orangi et al., 2011; Chaudhary, 2011; Honarpour et al., 2012). Table 13 lists these reservoir simulation parameters.

Table 13: Model I reservoir simulation parameters.

Parameter	Value
Matrix porosity ( $\emptyset$ ), fraction	0.06
Matrix permeability in all directions ( $K_{i,j,k}$ ), nd	200
Depth to top of formation, ft	10,000
Pay zone thickness, ft	200
Initial reservoir pressure, psi	6,490
Depth of water oil contact, ft	15,000
Fracture spacing, ft	200
Reservoir rock compressibility, $\text{psi}^{-1}$	$10 \times 10^{-6}$
Minimum bottomhole flowing pressure, psi	1,000
Maximum surface liquid rate, STB/day	200

It must be mentioned again that this simulation model is for a single hydraulic fracture only. Therefore, all results, graphs and tables are for a single hydraulic fracture unless stated otherwise. A good estimate for total well production rate and cumulative production is to multiply the single hydraulic fracture results by the number of stages.

### 3.2.2 Fluid Model

The initial reservoir pressure in the Eagle Ford oil window is well above reservoir fluid bubble point pressure and makes the reservoir undersaturated. CMG-IMEX requires the input data listed in Table 14 to build a fluid model.

Table 14: Reservoir fluid properties (Chaudhary, 2011).

Parameter	Value
Reservoir temperature, °F	250
Bubble point pressure for oil, psi	2398
Solution gas oil ratio, SCF/STB	650
Oil ° API gravity	42
Under-saturated oil compressibility, psi <sup>-1</sup>	$1 \times 10^{-5}$
Gas specific gravity	0.8

Figures 22 and 23 present oil formation volume factor ( $B_o$ ), solution gas oil ratio ( $R_s$ ) and oil viscosity trends as a function of pressure.

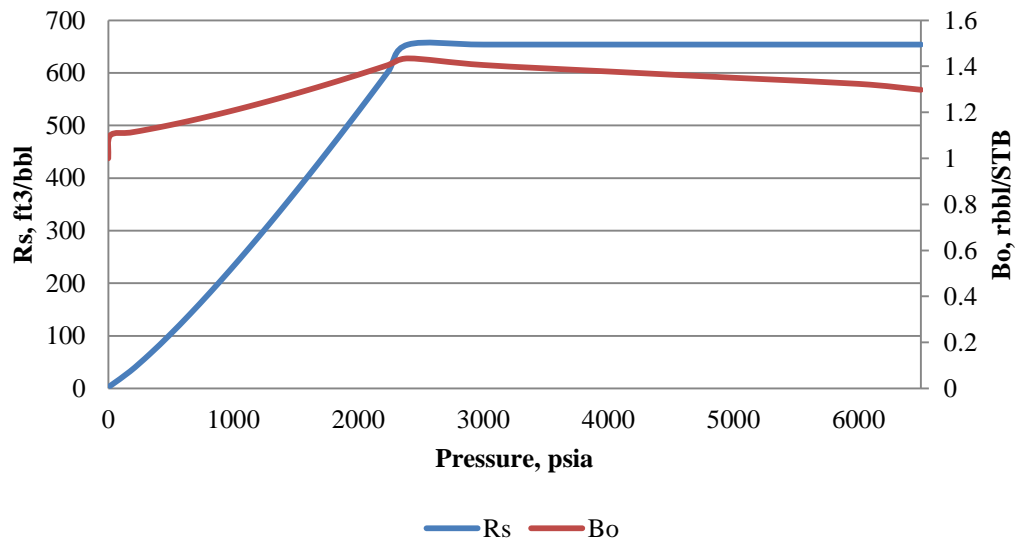


Figure 22: Oil formation volume factor (Bo) and solution gas oil ratio (Rs) as a function of pressure.

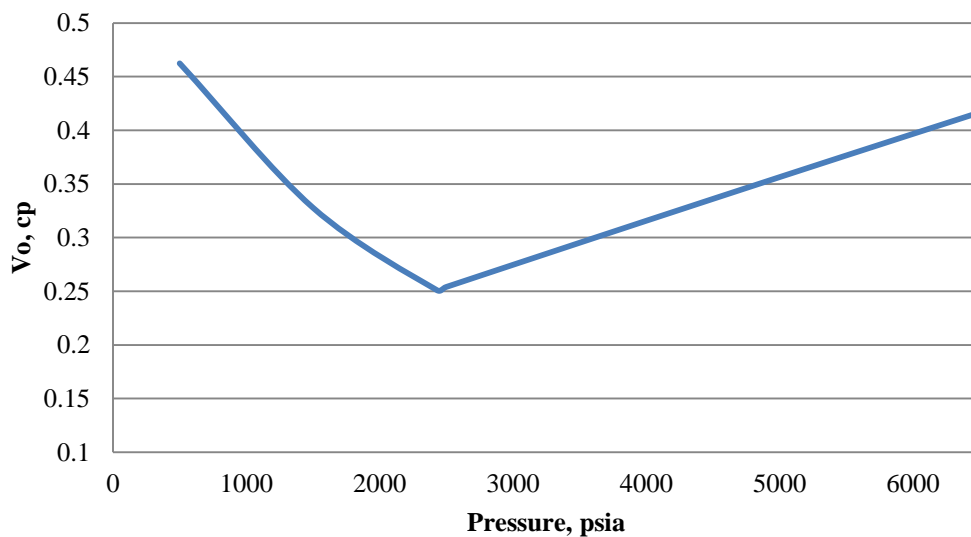


Figure 23: Oil viscosity trend versus pressure.

### 3.2.3 Relative Permeability Curves

Relative permeability curves used in simulations of matrix and fracture are generated using the Corey Model (1954), based on the end points developed by Honarpour et al. (2012) for the Eagle Ford Shale, listed in Table 15. They proposed end points for the TOC-rich matrix of the Eagle Ford Shale and hydraulic fractures. In general, the relative permeability endpoints are higher in the fracture compared to the matrix, providing a better flow path for the fluid. Another difference is that exponents are relatively lower for the fracture compared to the matrix, reducing the curvature and making the curves close to linear.

Figures 24 and 25 represent water-oil and liquid-gas relative permeability curves for a TOC-rich matrix and hydraulic fracture. Relative permeability curves for a hydraulic fracture follow an almost linear trend. Also, at a specific saturation, oil, gas, and water relative permeability values are higher in the hydraulic fracture compared to those in the matrix. These curves were used in building the simulation model in CMG-IMEX.

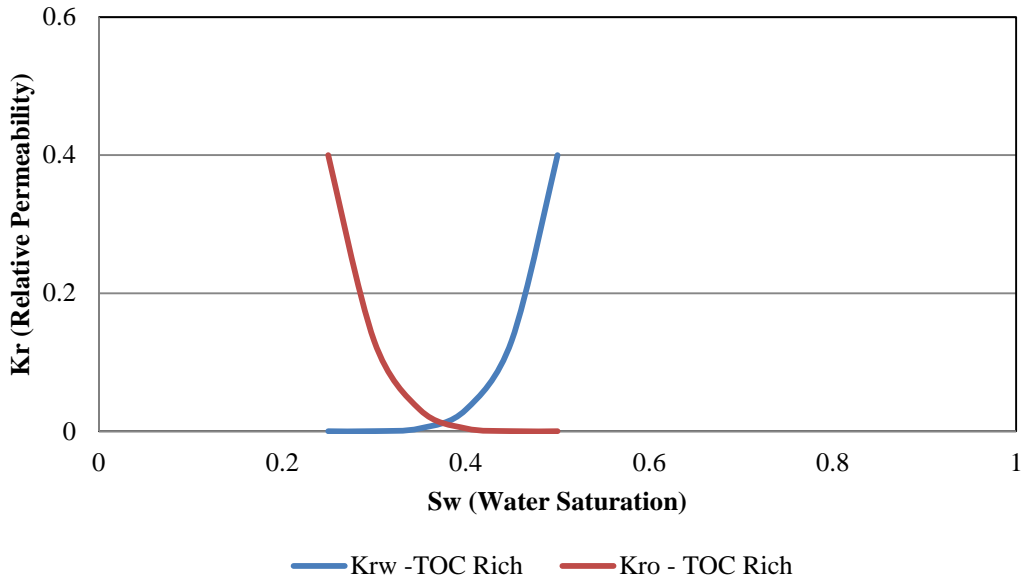
Below is the description of the parameters used in Table 15:

- $K_{ro}$ : Oil relative permeability
- $K_{rg}$ : Gas relative permeability
- $K_{rw}$ : Water relative permeability
- Corey O/W: Corey exponent for calculating  $K_{ro}$  in water-oil relative permeability curve
- Corey O/G: Corey exponent for calculating  $K_{ro}$  in gas-liquid relative permeability curve
- Corey Gas: Corey exponent for calculating  $K_{rg}$

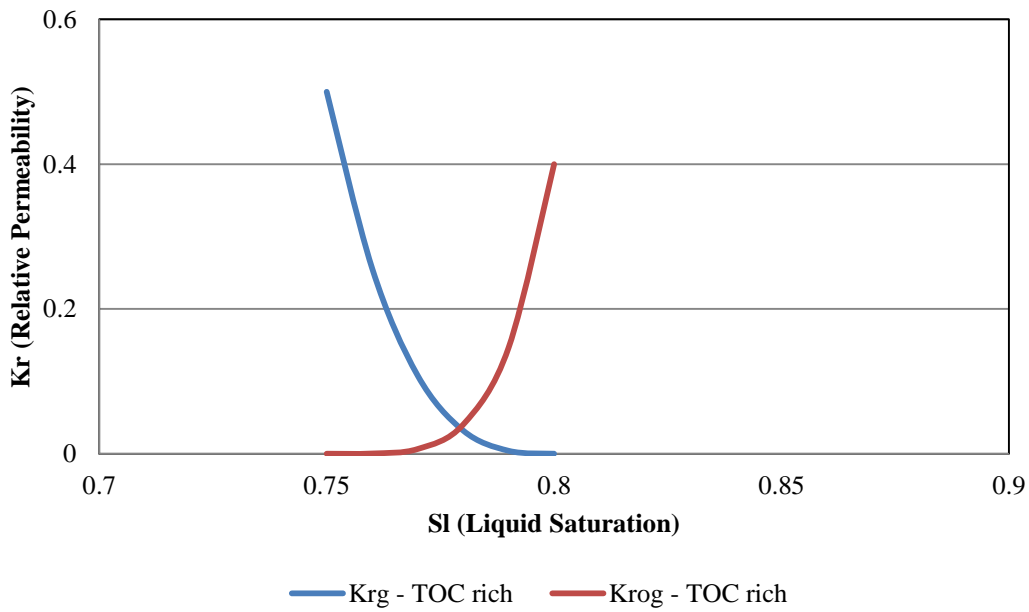
- $S_{wi}$  or  $S_{wmin}$ : Initial water saturation (connate water saturation)
- $S_{wcr}$ : Critical water saturation
- $S_{org}$ : Residual oil saturation
- $S_{gc}$ : Critical gas saturation.

Table 15: Relative permeability models for the Eagle Ford developed by Honarpour et al. (2012).

	Gas Phase		Oil Phase		Water Phase	
<b>TOC-rich</b>	$S_{gc}$	0.2	$S_{org}$	0.5	$S_{wmin}$	0.25
	<b>Corey Gas</b>	3	<b>Corey O/W</b>	5	$S_{wcr}$	0.25
	$K_{rg}$ at $S_{wmin}$	0.5	<b>Corey O/G</b>	4.5		
	$K_{rg}$ at $S_{org}$	0.01	$K_{ro}$ at $S_{omax}$	0.4		
	Gas Phase		Oil Phase		Water Phase	
<b>Fracture</b>	$S_{gc}$	0.05	$S_{org}$	0.1	$S_{wmin}$	0.1
	<b>Corey Gas</b>	1.2	<b>Corey O/W</b>	2.5	$S_{wcr}$	0.1
	$K_{rg}$ at $S_{wmin}$	0.9	<b>Corey O/G</b>	1.5		
	$K_{rg}$ at $S_{org}$	0.05-0.5	$K_{ro}$ at $S_{omax}$	0.7		

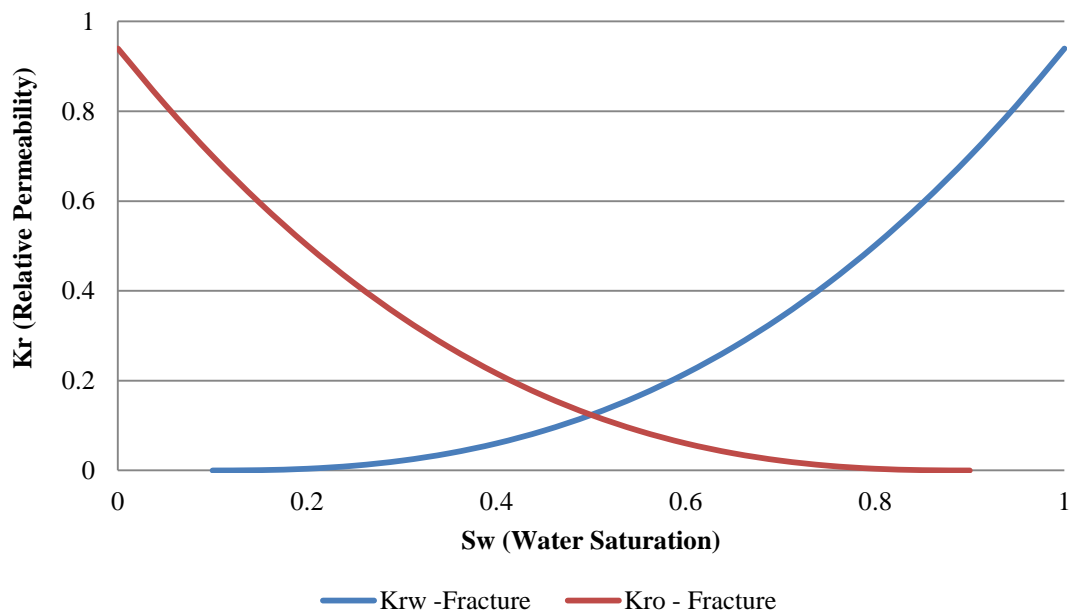


(a)

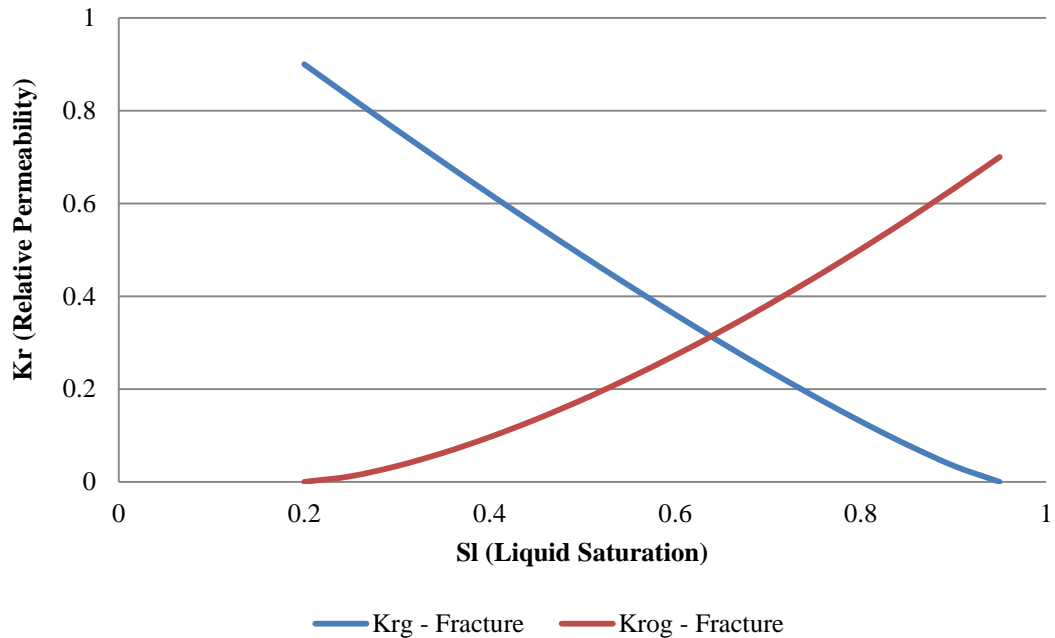


(b)

Figure 24: (a) Water-oil relative permeability curve for TOC-rich matrix. (b) Liquid-gas relative permeability curve for TOC-rich matrix.



(a)



(b)

Figure 25: (a) Water-oil relative permeability curve for hydraulic fracture blocks. (b) Liquid-gas relative permeability curve for hydraulic fracture blocks.



### 3.2.4 Fracture Closure

Reservoir pressure decrease during depletion can result in rock and proppant compaction, which can reduce matrix and fracture permeability (Warpinski, 2009). While this effect is negligible for matrix, it can greatly impact hydraulic fracture performance. The fracture closure effect is applied in the simulation model by using pressure-dependent permeability multipliers for hydraulic fracture grid blocks generated by Fracpro (Figure 26). For example, hydraulic fracture permeability decreases by 50% when reservoir pressure drops from an initial value of 6500 psi to 5000 psi.

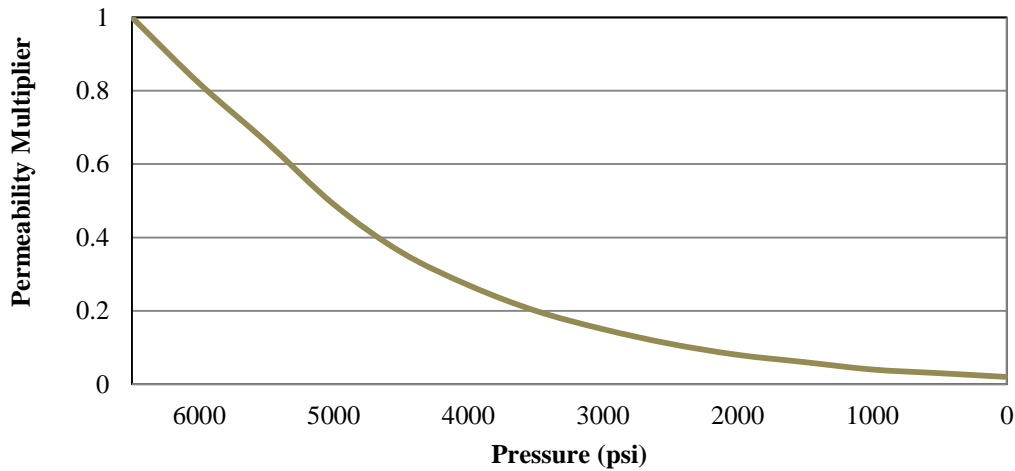


Figure 26: Pressure-dependent permeability multipliers for hydraulic fracture blocks.

### 3.3 Model II

As mentioned earlier, during hydraulic fracture treatment, fracturing fluid, mainly water, is injected into a formation. Clarkson and Kovacs (2013) presented a conceptual model for fluid flow in a hydraulic fracture, shown in Figure 27. At the start of production, some of the fracturing fluid stored in the hydraulic fracture is produced. There is no formation fluid production at this stage (Figure 27(a)). As time passes, formation fluid breakthrough occurs. Formation fluid flows initially into the hydraulic fracture, then into the wellbore (Figure 27(b)). An efficient simulation model should consider this effect.

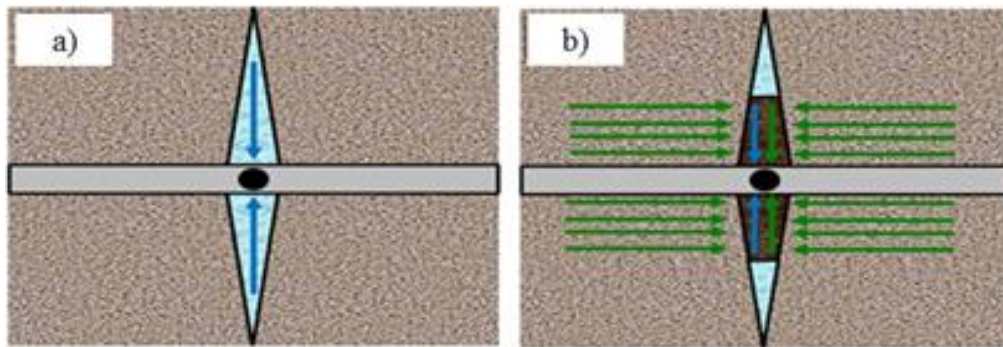


Figure 27: Conceptual model of flowback before and after breakthrough of formation fluid. (a) Fracturing fluid (blue arrows) production at early production time. (b) Breakthrough of formation fluid (green arrows) (Clarkson and Kovacs, 2013).

Another important matter is permeability distribution in hydraulic fracture blocks. In Model I, a constant permeability value was assumed for all hydraulic fracture cells, while, as shown in Figure 19 - stage 9, hydraulic fracture permeability varies greatly depending on proppant concentration.

Model I is modified to Model II in order to account for the presence of fracturing fluid in a hydraulic fracture prior to production, as well as permeability variation in the hydraulic fracture plane. All other simulation parameters remain similar to those of Model I. The

procedure to build Model II consists of two steps. In the first step, hydraulic fracture propagation stages and conductivity profiles for a typical pumping schedule of slickwater hydraulic fracturing are generated using the fracturing design software Fracpro (section 3.1). In the second step, the results of the hydraulic fracturing design are incorporated into a single stage hydraulic fracture model in CMG-IMEX. Water is also injected into the simulation model, according to the pumping schedule, to account for the presence of fracturing fluid in the hydraulic fracture and its surrounding matrix prior to commencing production. Before simulating production, the well is shut in for some time, to mimic the practice in the field (Zanganeh et al., 2014).

### **3.3.1 Incorporating Fracpro Results into the CMG-IMEX**

Fracture propagation stages generated by Fracpro were incorporated into the simulation software in nine steps in order to mimic actual fluid injection and oil displacement into the matrix during hydraulic fracturing. In addition, at each step, a specified amount of water was injected according to the pumping schedule shown in Table 12. Figure 28 shows a side view of half of the simulation model at the fracture plane during treatment, based on generated propagation stages (the fracture is symmetrical, therefore, both halves are identical).

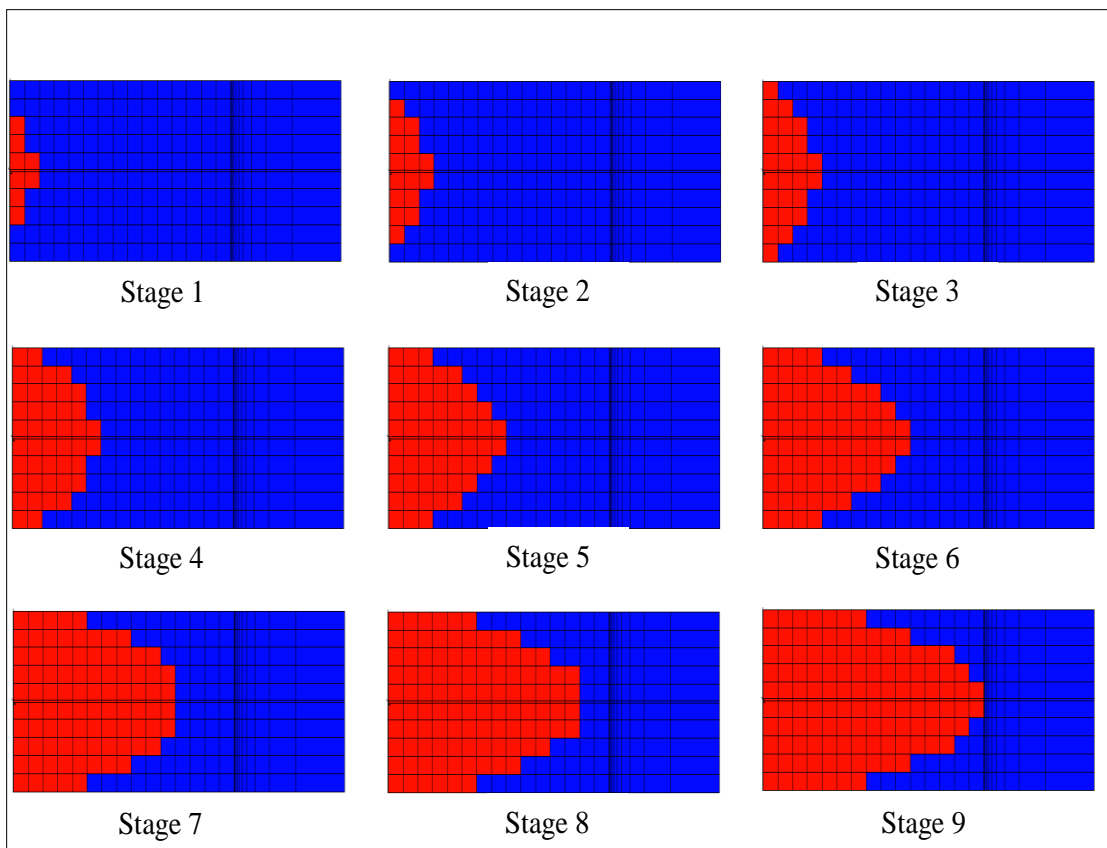


Figure 28: Side view of half of Model II at the fracture plane after fracture propagation stages imported into the reservoir simulation software. Red blocks represent hydraulic fracture and blue blocks represent matrix. At each stage water is injected into the model according to the pumping schedule.

The post-fracturing simulation model was built based on the conductivity profile of the last stage (Figure 19- stage 9). Figure 29(a) shows a side view of the post-fracturing simulation model parallel to the hydraulic fracture plane, based on the final stage conductivity profile. Figure 29 compares the permeability distribution at hydraulic fracture cells in Model I and Model II.

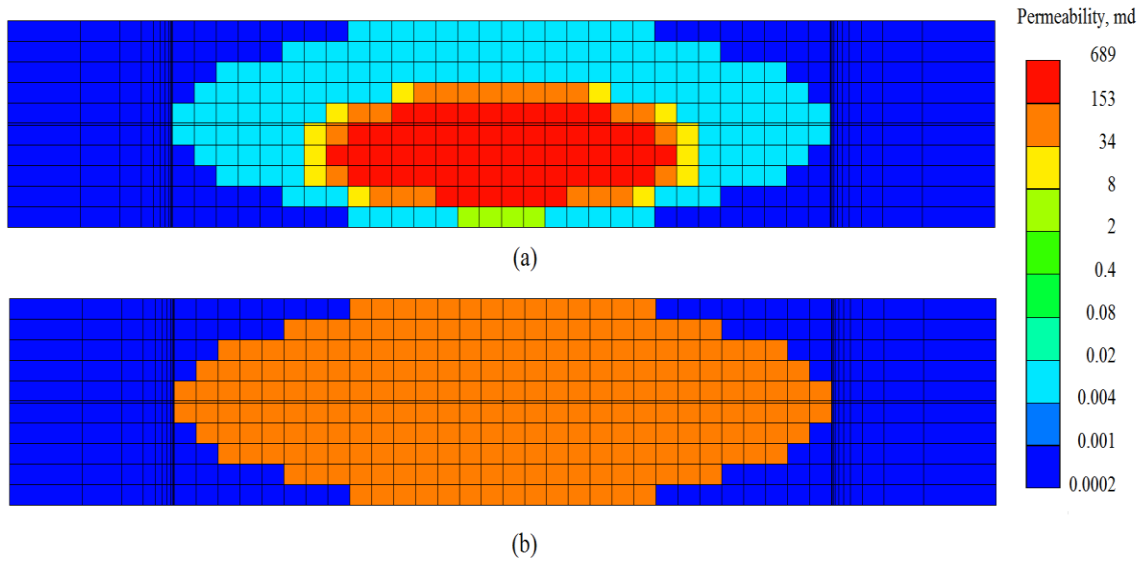


Figure 29: Side view of simulation models showing permeability distribution at the start of production. (a) Model II, where the permeability distribution is based on the last stage of hydraulic fracturing. (b) Model I, where permeability in fracture blocks remains constant, equal to the average values shown in (a).

Similarities and differences between Model I and Model II are summarized in Table 16. Model dimensions, hydraulic fracture geometry, hydraulic fracture half-length, hydraulic fracture height, and all matrix and fluid parameters are the same for the two models. There are only two differences between the two cases: the hydraulic fracture permeability distribution and the presence of fracturing fluid in matrix and hydraulic fracture prior to commencing production.

Table 16: Comparison of Model I and Model II

	<b>Model I</b>	<b>Model II</b>
<b>Dimension (height, thickness, length)</b>	Similar	Similar
<b>Fracture geometry (half length, height)</b>	Similar	Similar
<b>Fluid model</b>	Similar	Similar
<b>Relative permeability curves</b>	Similar	Similar
<b>Matrix properties ( porosity, permeability)</b>	Similar	Similar
<b>Production constraints</b>	Similar	Similar
<b>Fracture permeability/conductivity</b>	Constant average value (106 md)	Distributed according to proppant concentration ( 0.01 md – 600 md)
<b>Presence of fracturing fluid prior to production</b>	Ignored	Included by injection of water into the model



## Chapter 4 Results and Discussion

In this chapter, simulation results for Model I and Model II (described in the previous chapter) are provided. The original oil in place (OOIP) for both cases is 290,000 STB.

### 4.1 Model I

Figure 30 shows the oil production rate and cumulative oil production of Model I for 30 years of production. The maximum production rate constraint for a single hydraulic fracture is 200 STB/day. The maximum production rate sustains for 2 days, followed by a sharp decline that reduces the production rate to 10 STB/day within six months. The rate of decline progressively decreases. The production rate at the end of 30 years is around 1.00 STB/day. Since it was assumed that initial water saturation is equal to connate water saturation, the water production rate is equal to zero throughout the production period. The oil recovery factor after 30 years is 8% for Model I.

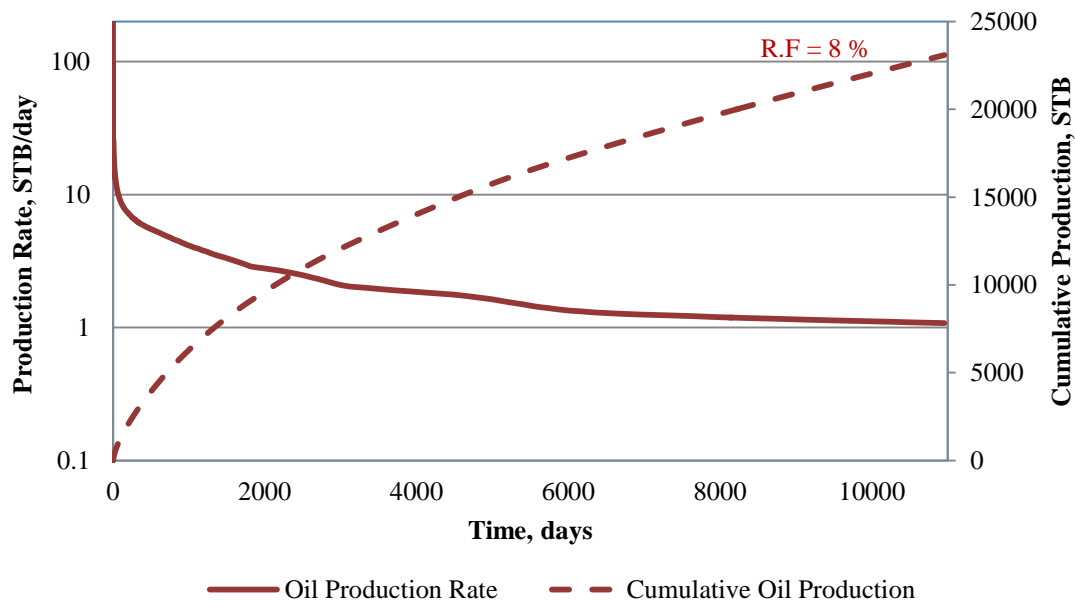


Figure 30: Oil production rate and cumulative oil production for Model I.



Figure 31 shows the producing Gas Oil Ratio (GOR) and average reservoir pressure versus time. The GOR remains almost constant during early production time. The variation in GOR, except for the first few days, is within 200 SCF/STB. The oscillations and wavy trend in the GOR curve are due to the size of the grid blocks. As production proceeds, the pressure depletion wave propagates away from fracture into larger grid blocks. The gas starts to come out of solution as soon as the average block pressure drops below bubble point pressure, but since depletion is slow, it takes some time for the gas saturation to reach its critical value and become mobile. This is when the GOR decreases. As soon as gas in the next block becomes mobile, the GOR increases. The cycle repeats as the depletion wave reaches each new cell. Average reservoir pressure decreases from an initial value of 6490 psi to 2600 psi during 30 years of production. If we use very small grid sizes (total number of 300,000 grid blocks), as shown in Figure 31 by the black curve, the amplitude of the wave decreases and the trend becomes almost linear. However, this approach increases the simulation time from hours to days, which is not efficient.

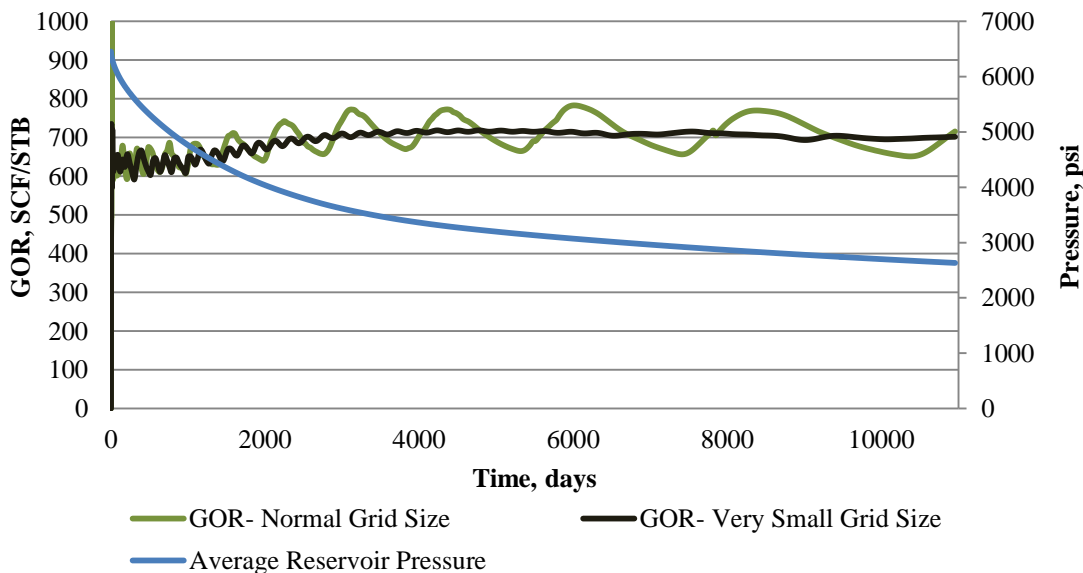
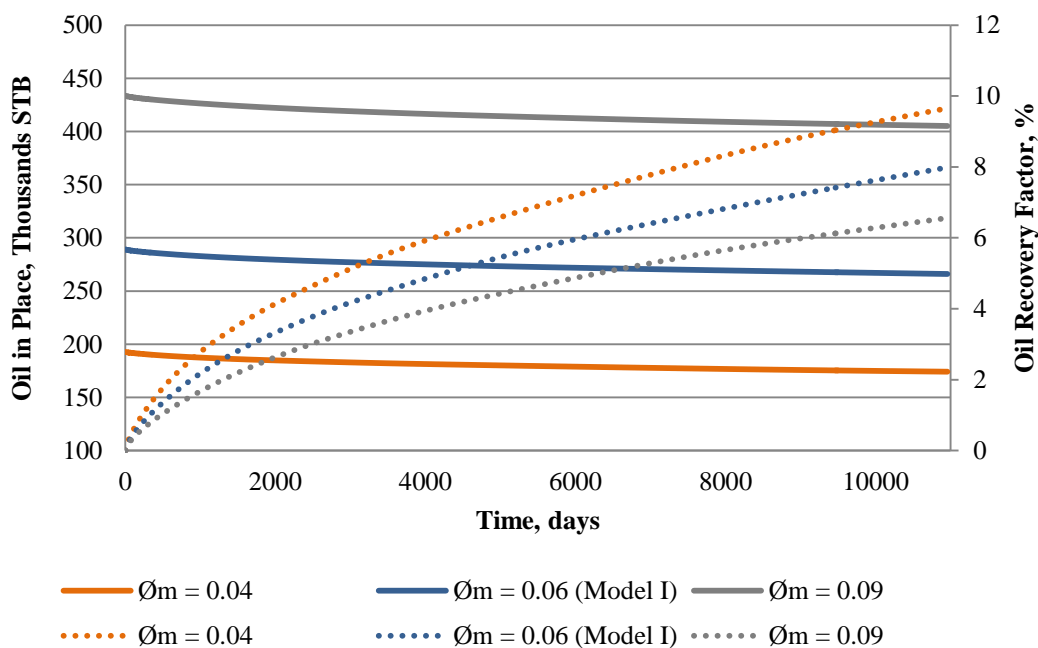


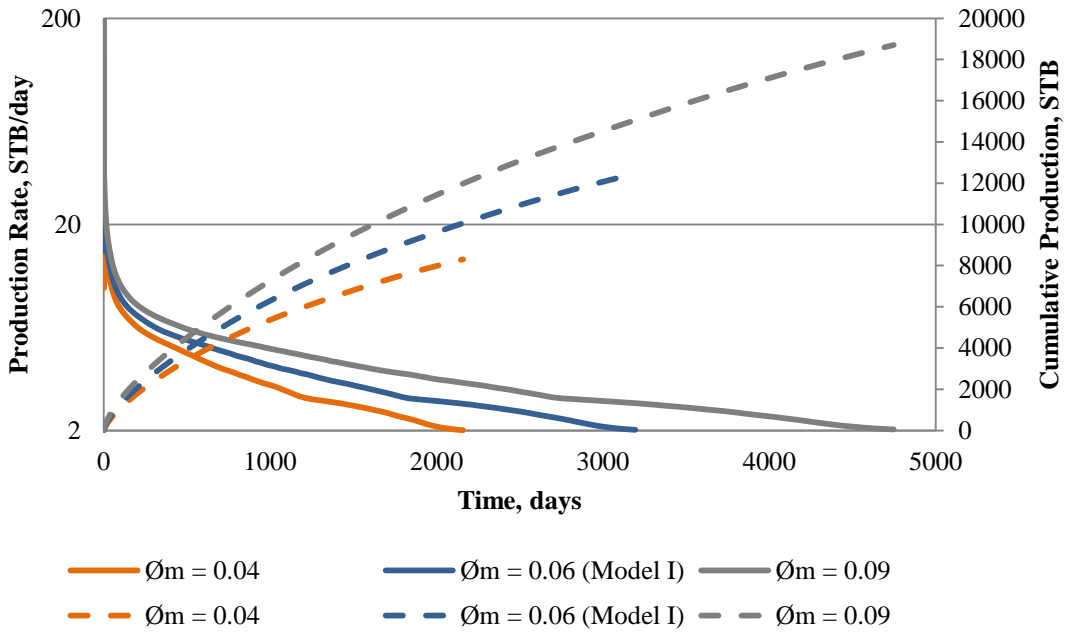
Figure 31: Producing GOR and average reservoir pressure for Model I during production time.

#### 4.1.1 Effect of Matrix Porosity and Permeability

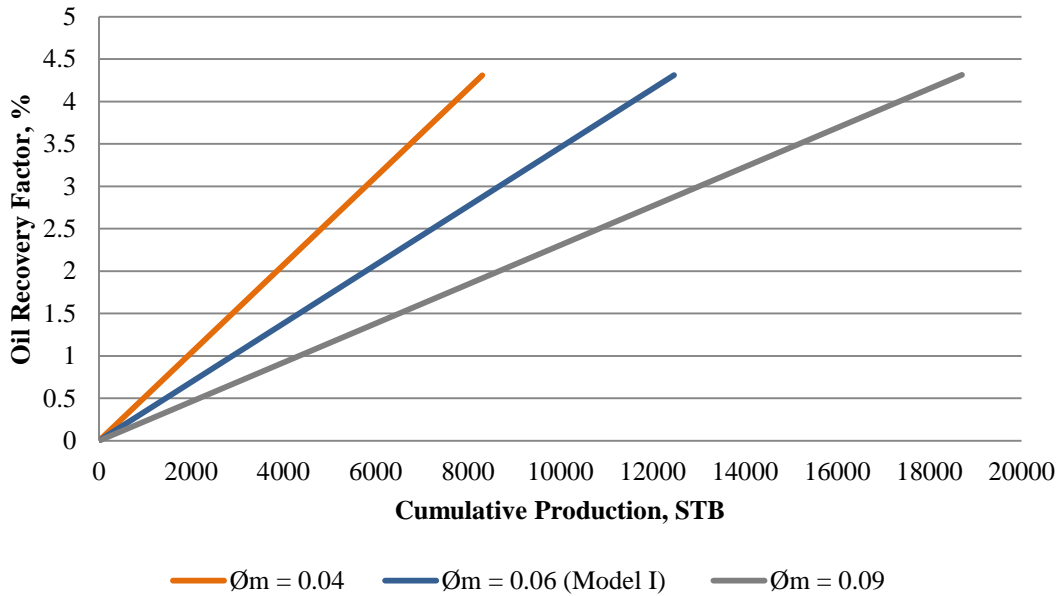
Figure 32(a) shows the effect of matrix porosity ( $\emptyset_m$ ) on the values of original oil in place (OOIP) and remaining oil volume during production. Matrix pore volume and OOIP increase as the matrix porosity increases; however, the oil recovery factor for 30 years of production falls behind as the matrix porosity increases (Figure 32(a)). At the same production time, as porosity increases the cumulative production increases, Figure 32(b), but the recovery factor is lower, Figure 32(c). In other word, as porosity increases the well needs more time to produce up to a given recovery factor. All wells produce to the same recovery factor down to a given production rate, Figure 32(b). For example as shown in Figure 32(b), producing down to minimum oil rate constraint of 2.0 STB/day, model with  $\emptyset_m = 0.04$  produces 8,000 STB and reaches there by 2,160 days while for a model with  $\emptyset_m = 0.09$  it takes 4,900 days and produces 18,500 STB. Recovery factor for these cases at the end of their respective production times is similar and equal to 4.3% (Figure 32(c)).



(a)



(b)



(c)

Figure 32: (a) Effect of matrix porosity on oil in place and recovery factor in Model I. (b) Oil production rate and cumulative oil production versus time when minimum production rate constraint is used. (c) Oil recovery factor versus cumulative oil production when minimum production rate constraint is used.

The oil recovery factor is significantly affected by matrix permeability, as shown in Figure 33. Higher matrix permeability results in higher oil recovery factor. For example, oil recovery factor for a matrix permeability of 5 nd is almost negligible (1.3%), while for a matrix permeability of 500 nd, it is 11.3%.

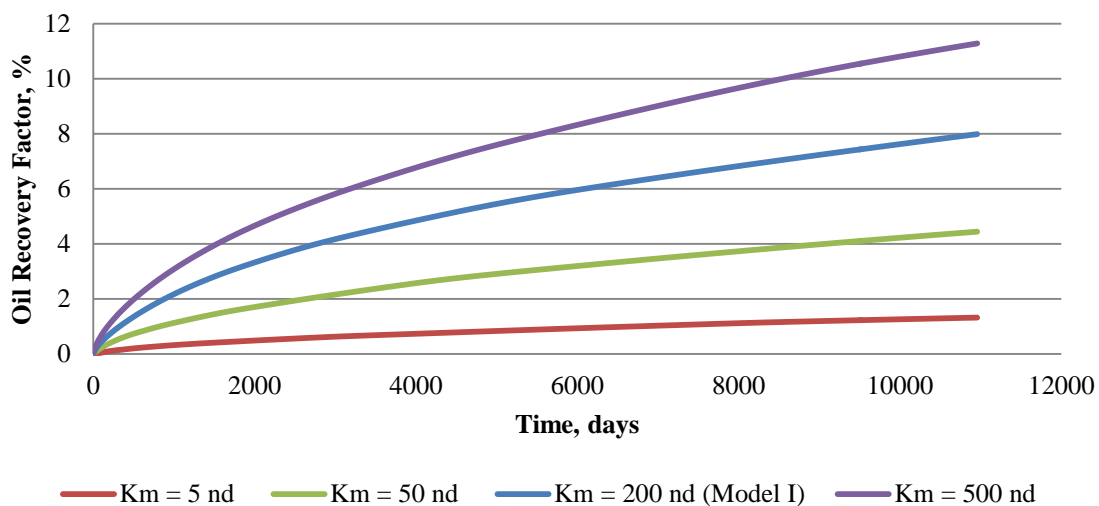


Figure 33: Effect of matrix permeability on oil recovery factor in Model I.

#### 4.1.2 Effect of Hydraulic Fracture Permeability

Figure 34 represents the effect of hydraulic fracture permeability on the oil recovery factor of Model I. The oil recovery factor increases as the hydraulic fracture permeability increases up to 500 md, with negligible increase beyond that. In this permeability range, the hydraulic fracture is assumed to be infinitely conductive, and further increases in its permeability do not affect well performance.

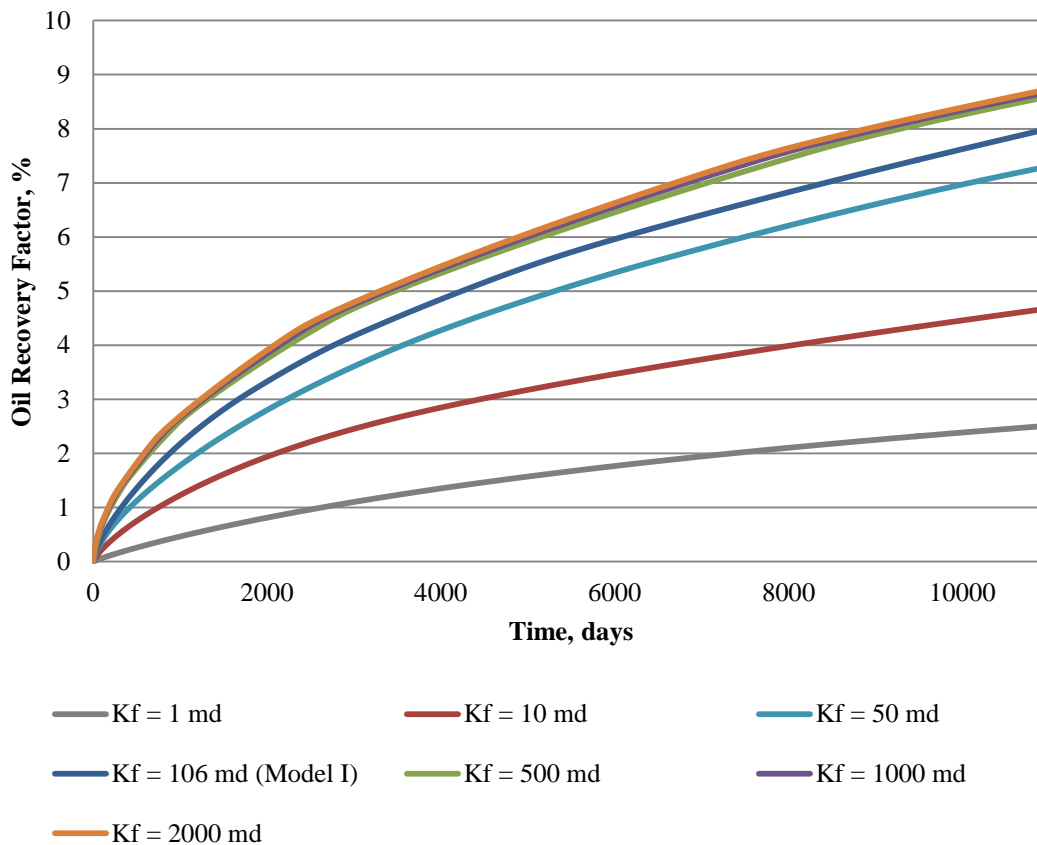


Figure 34: Effect of hydraulic fracture permeability on oil recovery factor in Model I.

### 4.1.3 Effect of Fracture Closure

The effect of fracture closure during depletion was considered for all models. In order to observe the effect of fracture closure on production performance, a simulation run was conducted on Model I without considering this effect. Figure 35 summarizes the oil recovery factor for these two cases. Ignoring the fracture closure effect in the simulation model resulted in overestimation of the oil recovery factor by as much as 10 %.

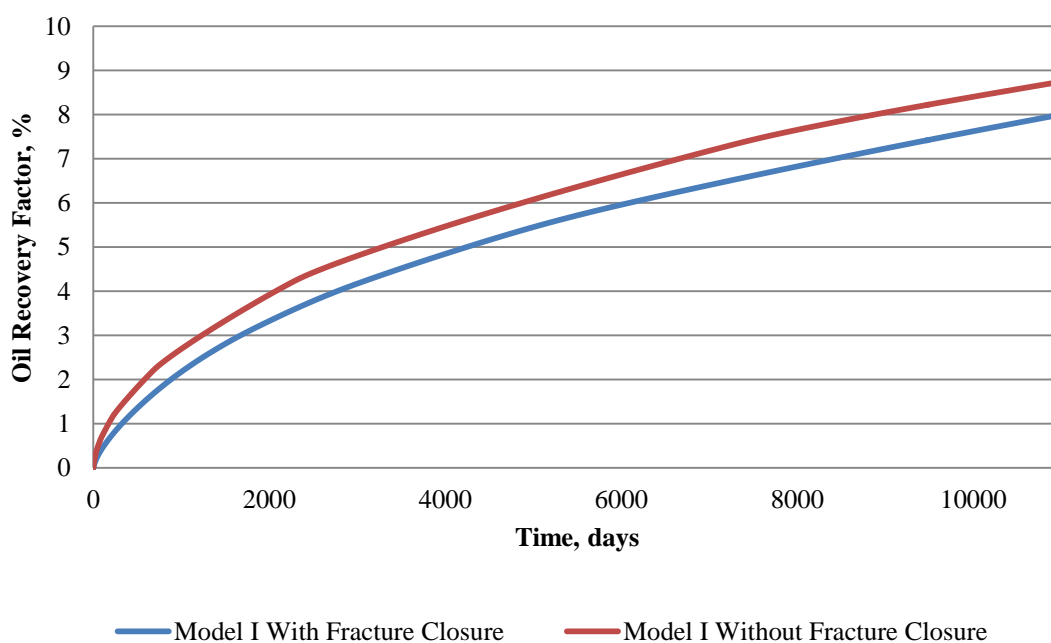


Figure 35: Effect of fracture closure during depletion on oil recovery factor in Model I.

## 4.2 Model II

### 4.2.1 Injection Profiles during Treatment

Water, the main component of fracturing fluid, is injected into the simulation Model II according to the pumping schedule, to account for the presence of fracturing fluid in the hydraulic fracture and in the matrix around it prior to commencing production. Figure 36 shows the fracturing fluid (water) injection rate and cumulative injection profiles for Model II. A total of 1,170 barrels of water is injected into the single fracture/formation during 26 minutes of fracturing treatment, with the injection rate held constant at 45 bpm. The average pressure at the end of injection was 6,605 psia.

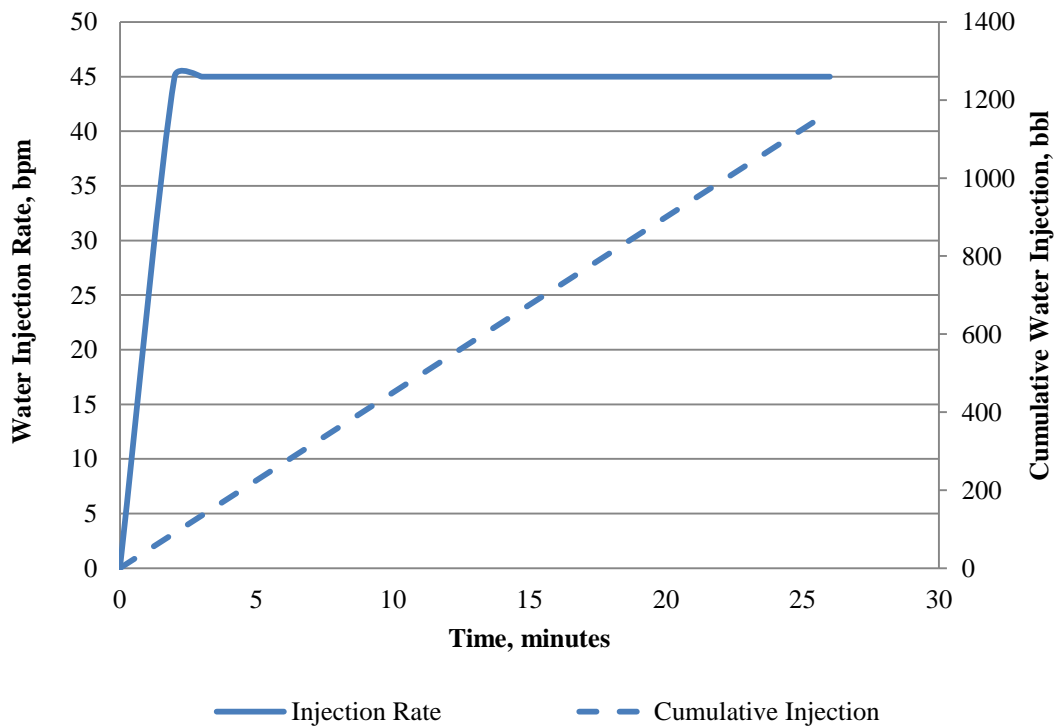


Figure 36: Water injection profile in Model II.

#### 4.2.2 Production Trends

Oil and water production profiles for 30 years of production in Model II are presented in Figure 37. For better resolution, only the first year of production is shown in Figure 38. Production starts initially with 100% water production at maximum wellhead flow rate. This can be interpreted as reflecting the production of the fracturing fluid stored in the hydraulic fracture. Water production decreases; after few days, oil/gas breakthrough occurs, and oil production begins and increases as water production continues to decline. The oil production rate reaches its maximum value of 10 STB/day after almost sixty days, then declines. Figure 39 represents the cumulative oil production and recovery factor for Model II. The oil recovery factor after 30 years of production for Model II is 5.8 %.

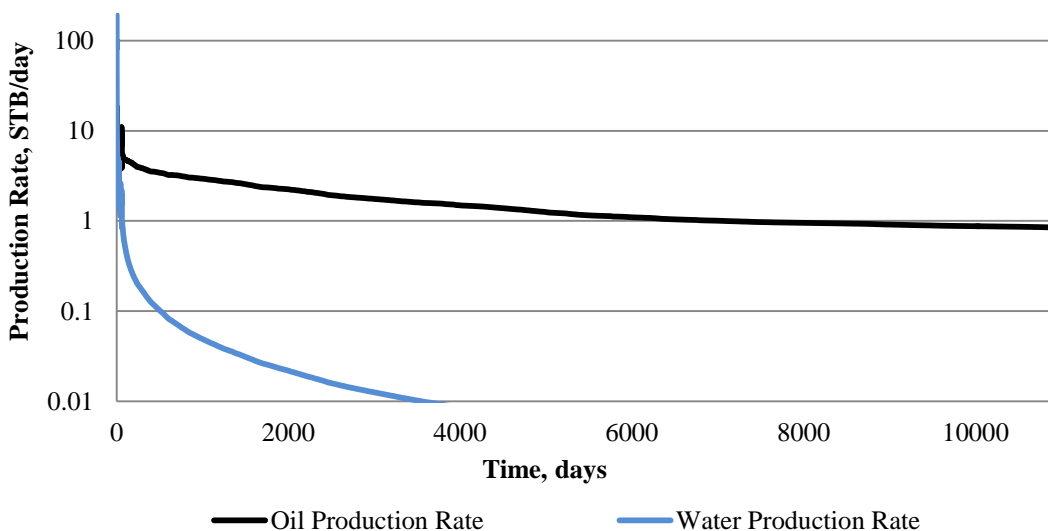


Figure 37: Oil and water production trends during 30 years of production in Model II.



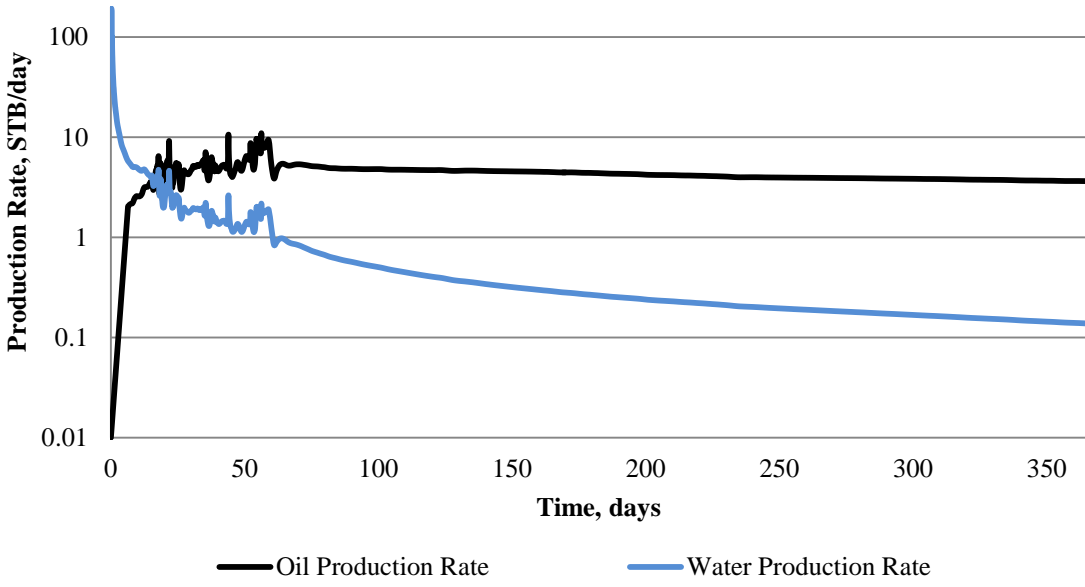


Figure 38: Oil and water production trends during first year of production in Model II.

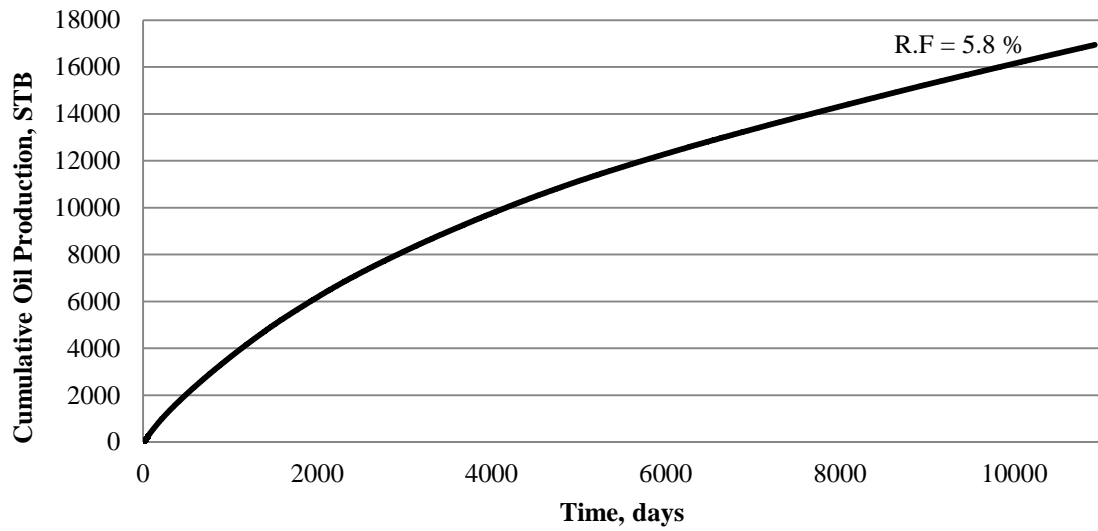


Figure 39: Cumulative oil production and recovery factor for Model II.

### 4.2.3 Effect of Fracturing Fluid Flowback

In order to observe the effect of flowback and water production on oil recovery in Model II, a simulation run was performed on the same model but without injecting water prior to production. Figure 40 shows the difference in oil production trends for both cases. For better resolution, only production rates for the first year are presented.

As discussed before, the general trend for oil production, considering flowback in Model II, is a low initial production rate, followed by an increase to a maximum value, followed by a decline (black curve in Figure 40). However, as shown by the red curve in Figure 40, ignoring the initial presence and production of water results in a high initial oil production rate. The oil production profiles and cumulative production for 30 years of production for these two cases are presented in Figure 41. Ignoring flowback and water production results in overestimating the recovery factor by 17 % in Model II.

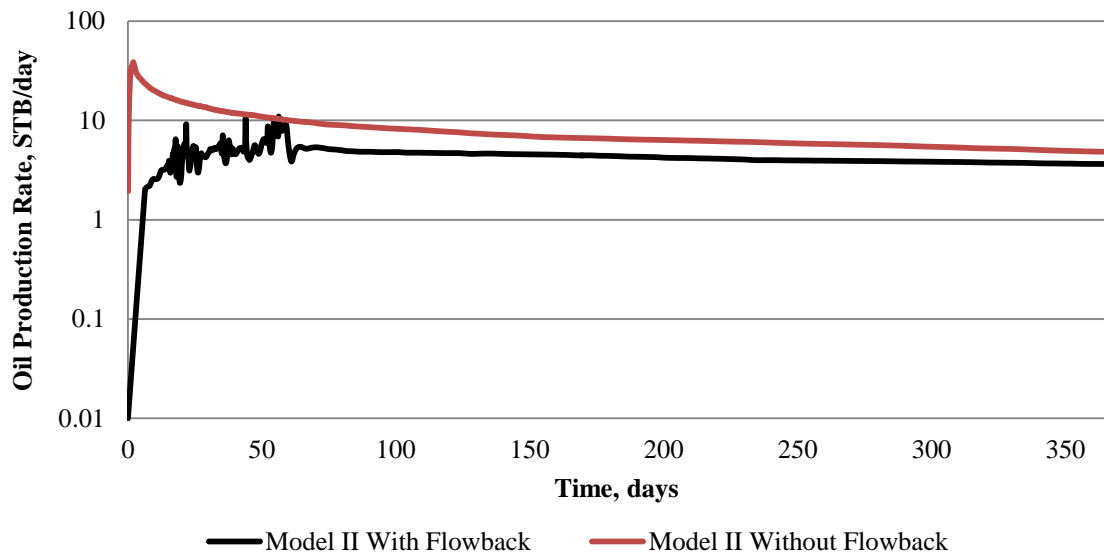


Figure 40: Oil production trend with and without considering fracturing fluid (water) flowback in Model II.

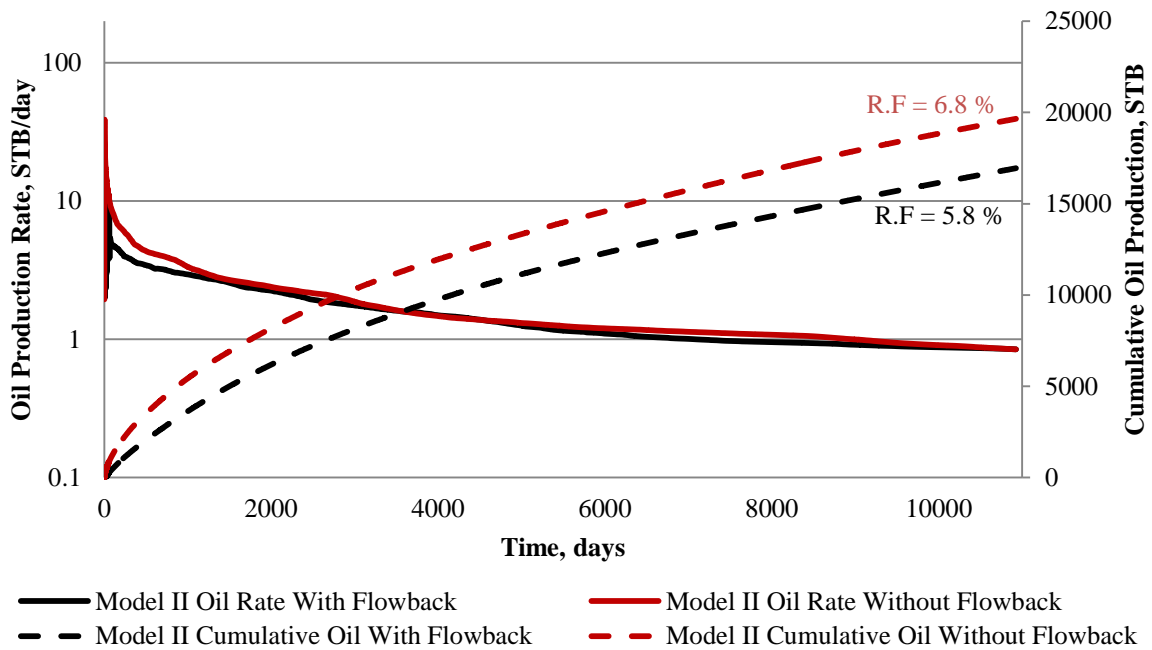


Figure 41: Comparison of cumulative oil production with and without considering fracturing fluid (water) flowback in Model II.

#### 4.2.4 Fracturing Fluid Recovery

Figure 42 shows the simulated flowback of fracturing fluid (water) over 30 years of production in Model II. Over 30 years, 518 barrels of water (out of 1170 barrels injected) were recovered. Figure 43 shows fracturing fluid recovery as a percentage of the total 518 barrels recovered. Most of the fracturing fluid recovery occurs during the first year of production (74%), particularly the first 2 months of production (56%).

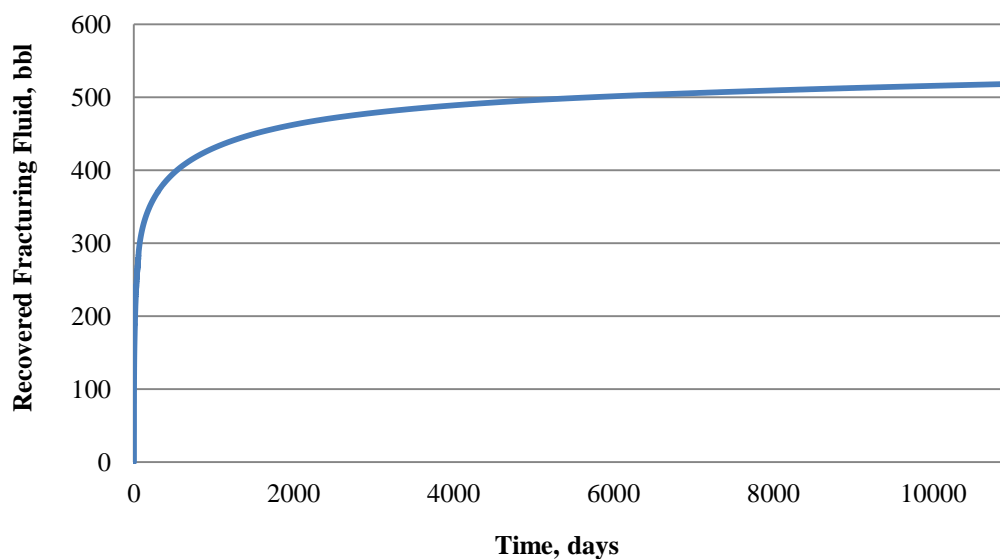


Figure 42: Amount of recovered fracturing fluid (water) during 30 years of production time in Model II.

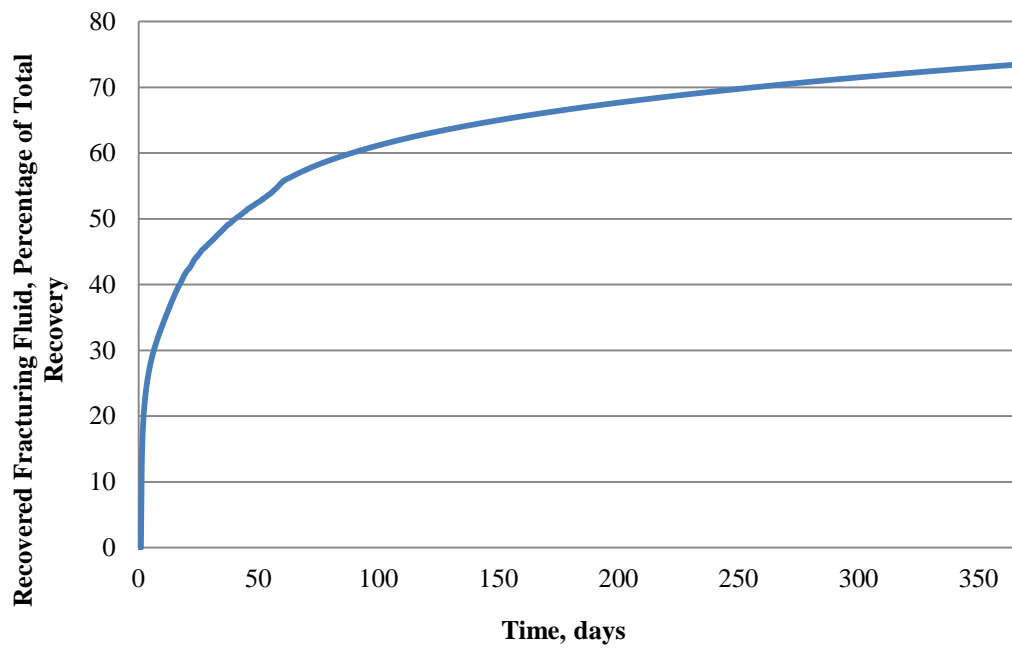


Figure 43: Recovered fracturing fluid (water) during the first year of production as a percentage of total recovery during 30 years.

#### 4.2.5 Effect of Unpropped Zone Conductivity on Production Performance

Fracpro, the fracturing design software used in this study, does not generate a conductivity value for the unpropped zone. In order to observe the effect of unpropped zone conductivity on production performance, simulation runs were conducted by assigning various permeability values, ranging from 0.0002 md (as low as matrix permeability) to 1 md (minimum permeability of hydraulic fracture in propped region), to grid blocks representing the unpropped region in Model II. The recovery factor increases as the permeability of the unpropped zone increases (Figure 44). For example, after 30 years, the recovery factor for Model II with unpropped zone permeability = 0.01 md is 5.8%, while for the model with unpropped zone permeability = 0.1 md, the recovery factor increases to 6.6 % (14% increase); for a model with unpropped zone permeability = 0.001 md, the recovery factor is reduced to 4.9 % (15% decrease). The difference in recovery factors becomes larger as production time increase. In low values of unpropped zone permeability, further permeability reduction due to fracture closure during production results in reduced contribution of this zone to fluid flow.

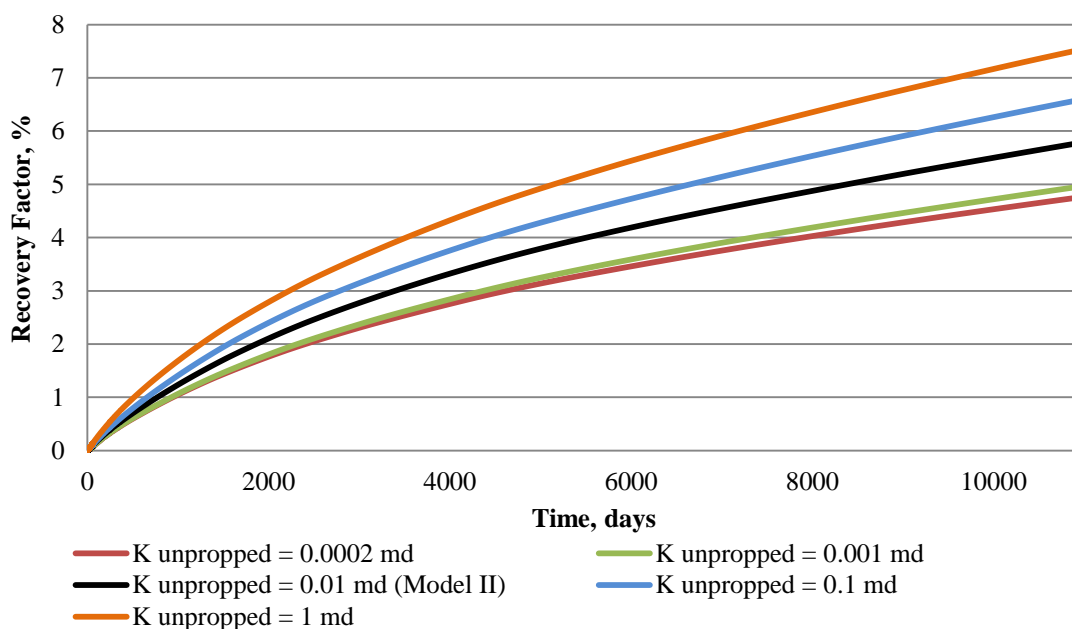


Figure 44: Effect of unpropped zone permeability on the oil recovery factor in Model II.

#### 4.2.6 Effect of Hydraulic Fracture Conductivity Profile on Production Performance

Figure 45 compares the oil recovery factors for two approaches to modeling hydraulic fracture permeability, as discussed in section 3.3 and Figure 29. The black curve shows the recovery factor for Model II that used the permeability distribution generated by the fracturing design software; the green curve represents the recovery factor for the model that used a constant permeability value equal to the average value of generated permeability distribution (106 md). As seen in Figure 45, assuming a constant permeability in the fracture plane overestimates the recovery factor by approximately 25% (1.5% of the total oil in place around single fracture). By assuming a constant permeability in the fracture plane, the difference in conductivity between the propped zone and the unpropped zone is ignored, meaning that a larger fracture plane contributes to fluid flow. This results in an overestimation of the recovery factor.

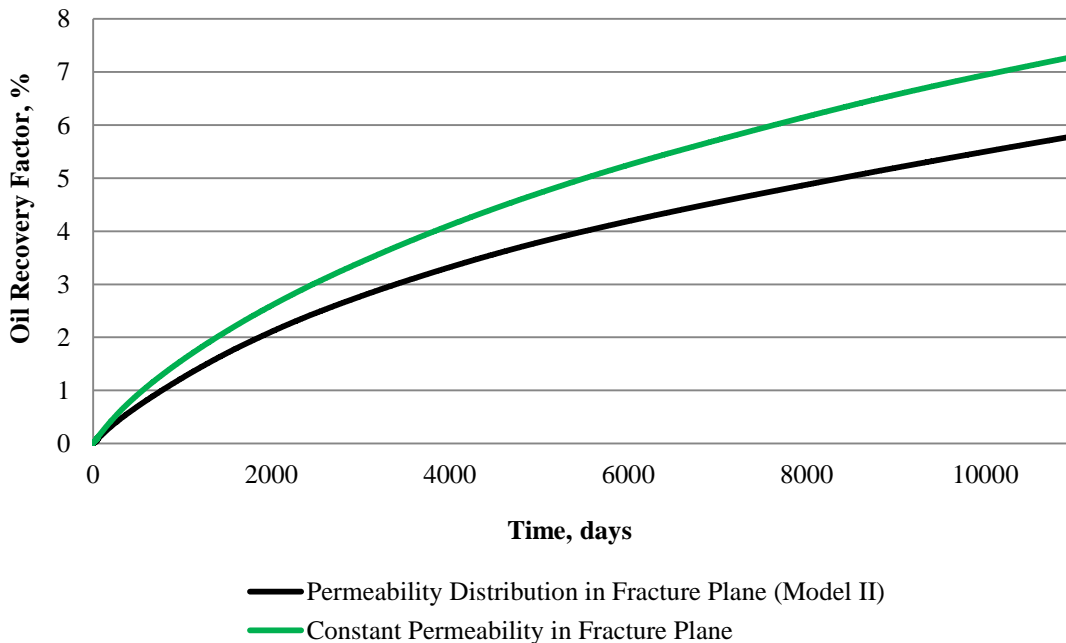


Figure 45: Comparison of oil recovery factor for two approaches in modeling of fracture conductivity/permeability in Model II.

#### 4.2.7 Effect of Permeability Anisotropy

Shale is laminated, meaning that the rock is made up of many thin layers (Mohaghegh, 2013). This characteristic may result in lower matrix vertical permeability ( $K_v$ ) than horizontal permeability ( $K_h$ ). In Model II, it was assumed that vertical and horizontal permeabilities are equal ( $K_v/K_h=1$ ). In order to observe the effect of permeability anisotropy on the oil recovery factor, a simulation run was performed on Model II, with  $K_v/K_h = 0.1$ . Figure 46 summarizes the oil recovery factor for the two cases. The oil recovery factor decreases from 5.8% to 5.4% by assuming  $K_v/K_h = 0.1$ .

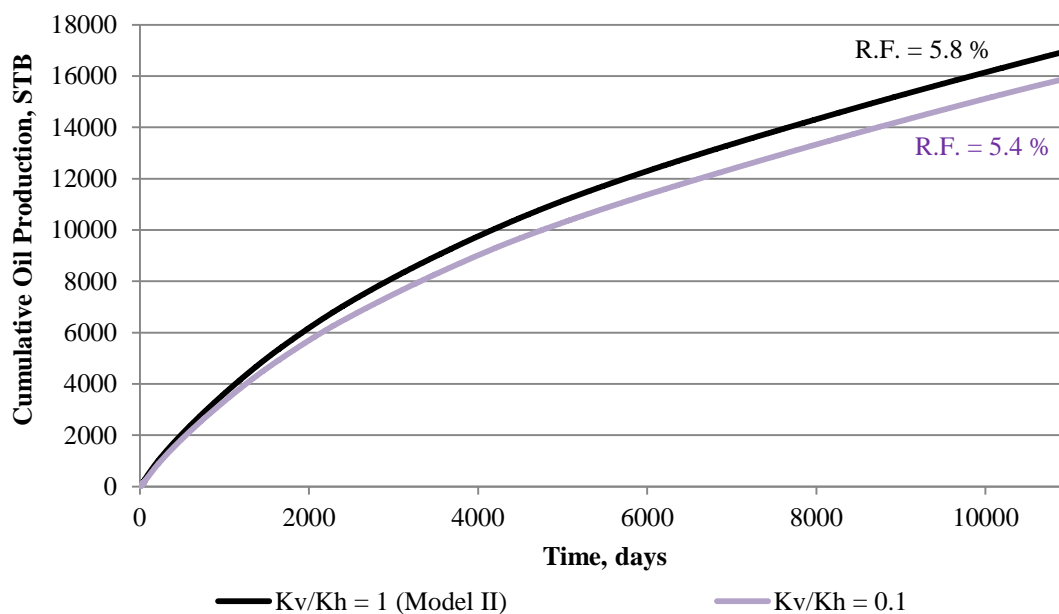


Figure 46: Effect of permeability anisotropy on production performance in Model II.





## Chapter 5 Conclusions and Recommendations

### 5.1 Conclusions

Two simulation models were presented for a single shale oil well in a typical carbonate-rich shale formation, such as the Eagle Ford, in order to study well performance and identify the parameters affecting it.

Model I was built assuming a constant permeability in hydraulic fracture cells. Model I ignores the presence of fracturing fluid in the hydraulic fracture and its surrounding matrix prior to production. This simple approach allows studying the effects of different parameters such as shale porosity and permeability, as well as hydraulic fracture conductivity and closure, on production performance in a reasonable time.

Oil production in Model I commences with the maximum wellhead flow rate of 200 STB/day followed by a sharp decline that reduces the production rate to 10 STB/day within six months. The oil recovery factor for Model I after 30 years is 8%. The GOR remains almost constant at 650 SCF/STB during early production time and increases to 700 SCF/STB toward the end. The oil recovery factor progressively decreases from 9.6% to 6.9 % with an increase in porosity from 4% to 8%. Matrix permeability is one of the most important factors affecting oil recovery. The oil recovery factor increases from 4.4% to 11.2% by changing matrix permeability from 50 md to 500 md. The oil recovery factor remains practically unchanged for an infinitely conductive hydraulic fracture ( $K_f > 500$  md) and decreases as fracture permeability drops below 500 md. This suggests that ignoring the fracture closure effect in the simulation model results in overestimation of the oil recovery factor by as much as 10 % (8.0% versus 8.8%).

Model II was developed to consider permeability variation in hydraulic fracture cells and to account for the presence of fracturing fluid in the hydraulic fracture and surrounding matrix prior to production. All other simulation parameters remained similar to those of Model I.

Model II initially produces 100% water at its maximum rate. Water production decreases quickly and, after a few days, formation fluid breakthrough occurs, in which oil production begins and increases as water production continues to drop. The oil production rate reaches its maximum value within 2 months and then begins to decline. The oil recovery factor for Model II is 5.8%. Ignoring the presence of fracturing fluid in Model II overestimates the oil recovery factor by almost 17% (6.8% versus 5.8%). Misrepresenting the permeability of the hydraulic fracture by using a constant average value overestimates the oil recovery factor by 25% (7.3 versus 5.8%). Simulations also indicated that, after 30 years of production, only a portion of the injected fracturing fluid was recovered (518 barrels of out of 1170 barrels injected). Most fracturing fluid recovery occurred during the first year (74%), particularly during the first 2 months of production (56%). Permeability anisotropy was found to affect the oil recovery factor. Decreasing the  $K_v/K_h$  ratio from 1 to 0.1 reduced the oil recovery factor from 5.8% to 5.4%. The recovery factor increased from 4.7% to 7.5% as the permeability of the unproped zone increased from 0.0002 md to 1 md.

The main advantage of the presented workflow is that it honors variable fracture conductivity, and presence of fracturing fluid in the fractures and surrounding matrix in simulation model. This approach is time consuming; therefore, might not be efficient in full-field simulation models where several multi staged hydraulically fractured horizontal wells are modeled.

## **5.2 Recommendations**

The reservoir simulation parameters used in this thesis were based on published data for the Eagle Ford Shale in Texas. To obtain more realistic results for the Shublik shale, it is recommended to conduct experiments on Shublik shale core samples and measure geomechanical and reservoir properties.

The presence of natural fractures can significantly affect the production performance of shale reservoirs. It is recommended to study the density and conductivity of natural fractures in the Shublik and consider them if they are important.

It was assumed that all hydraulic fracture stages are identical and contribute equally to fluid flow. If heterogeneity data and capable software are available, it is recommended to consider the heterogeneity of the reservoir and model several hydraulic fracture stages at the same time.

Reservoir simulation alone is not sufficient for determining the optimum development plan and number of hydraulic fracture stages. Economic analysis must be done parallel to reservoir simulation and fracturing design.



## References

Alkough, A., Schechter, D., Wattenbarger, R.A. 2012. Practical Use of Simulators for Characterization of Shale Reservoirs. Paper SPE 162645 presented at SPE Canadian Unconventional Resources Conference, Calgary, Alberta, Canada.

Cander, H. 2012. What Are Unconventional Resources? A Simple Definition Using Viscosity and Permeability?. Poster presented at AAPG Annual Convention and Exhibition, Long Beach, CA.

Chaudhary, A.S. 2011. Shale Oil Production Performance from a Stimulated Reservoir Volume. MS thesis, Texas A&M University.

Chaudhary, A.S., Economides, C.E., Wattenbarger, R.A. 2011. Shale Oil Production Performance from a Stimulated Reservoir Volume. Paper SPE 147596 presented at the SPE Annual Technical Conference and Exhibition, Denver, CO.

Chesapeake Energy 2012. Deep Shale Natural Gas and Water Use. [www.chk.com/Media/CorpMediaKits/Water\\_Use\\_Fact\\_Sheet.pdf](http://www.chk.com/Media/CorpMediaKits/Water_Use_Fact_Sheet.pdf)

Cipolla, C.L., Lolon, E.P., Mayerhofer, M.J., Warpinski N.R. 2009. The Effect of Proppant Distribution and Un-Propped Fracture Conductivity on Well Performance in Unconventional Gas Reservoirs. Paper SPE 119368 presented at the SPE Hydraulic Fracturing Conference, The Woodlands, TX.

Clarkson C.R., Williams-Kovacs, J.D. 2013. A New Method for Modeling Multi-Phase Flowback of Multi-Fractured Horizontal Tight Oil Wells to Determine Hydraulic Fracture Properties. Paper SPE 166214 presented at the SPE Annual Technical Conference and Exhibition, New Orleans, LA.

Corey, A.T., 1954. The Interrelation between Gas and Oil Relative Permeabilities. *Prod. Monthly*, 19 (1): 38.

Decker, P. L., 2012. Source-Reservoir Oil Resources, Alaskan North Slope. Presentation by Alaska Department of Natural Resources, Division of Oil and Gas.

EIA 2010. Eagle Ford Shale Play, Western Gulf Basin, South Texas. [http://www.eia.gov/oil\\_gas/rpd/shaleusa9.pdf](http://www.eia.gov/oil_gas/rpd/shaleusa9.pdf)

EIA 2011. Review of Emerging Resources: U.S. Shale Gas and Shale Oil Plays. Washington, DC. <http://www.eia.gov/analysis/studies/usshalegas/pdf/usshaleplays.pdf>

Environmental Protection Agency (EPA) 2010. Hydraulic Fracturing Research Study. <http://www.epa.gov/safewater/uic/pdfs/hfresearchstudyfs.pdf>

Friedrich, M. and Milliken, M. 2013. Determining the Contributing Reservoir Volume from Hydraulically Fractured Horizontal Wells in the Wolfcamp Formation in the Midland Basin. Paper SPE 168839/URTeC 1582170 presented at the 2013 Unconventional Resources Technology Conference, Denver, CO.

Holditch, S.S. 2003. The Increasing Role of Unconventional Reservoirs in the Future of the Oil and Gas Business. *Journal of Petroleum Technology*, 55(11): 34-38.

Honarpour, M.M., Nagarajan, N.R., Orangi, A., Arasteh, F., Yao, Z. 2012. Characterization of Critical Fluid, Rock, and Rock-Fluid Properties Impact on Reservoir Performance of Liquid-rich Shales. Paper SPE 158042 presented at the SPE Annual Technical Conference and Exhibition, San Antonio, TX.

Houseknecht, D. W., Rouse, W. A., Garrity, C. P. 2012a. Arctic Alaska Shale-Oil and Shale-Gas Resource Potential. Paper OTC 23796 presented at the Arctic Technology Conference, Houston, TX.

Houseknecht, D.W., Rouse, W.A., Garrity, C.P., Whidden, K.J., Dumoulin, J.A., Schenk, C.J., Charpentier, R.R., Cook, T.A., Gaswirth, S.B., Kirschbaum, M.A., Pollastro, R.M. 2012b. Assessment of Potential Oil and Gas Resources in Source Rocks of the Alaska

North Slope, 2012. USGS Fact Sheet 2012-13, [http://pubs.usgs.gov/fs/2012/3013/pdf/fs2012-3013\\_2-28-2012.pdf](http://pubs.usgs.gov/fs/2012/3013/pdf/fs2012-3013_2-28-2012.pdf)

Hulm, E.J. 1999. Subsurface Facies Architecture and Sequence Stratigraphy of the Eileen Sandstone, Shublik Formation, and Sag River Sandstone, Arctic Alaska. MS thesis, University of Alaska Fairbanks.

Hutton, E., Agboada, D. K., Whalen, M.T., Hanks, C.L. 2012. Upper Triassic Shublik Formation of North Alaska - An Eagle Ford Type Shale Reservoir Play?. Presented at AAPG Annual Convention and Exhibition. Long Beach, CA.

Hydraulic Fracturing Information Sheet 4, 2011. Hydraulic Fracturing: Treatment and Disposal of Fracking Fluid Waste.

[http://www.watershedcouncil.org/learn/hydraulic-fracturing/files/hydraulicfracturing information sheets/hydraulic fracturing and fracking fluid waste disposal.pdf](http://www.watershedcouncil.org/learn/hydraulic-fracturing/files/hydraulicfracturinginformation%20sheets/hydraulic%20fracturing%20and%20fracking%20fluid%20waste%20disposal.pdf)

Jackson, R., Pearson, B.R., Osborn S., Warner, N., Vengosh, A., 2011. Research and Policy Recommendations for Hydraulic Fracturing and Shale Gas Extraction. <http://www.nicholas.duke.edu/cgc/HydraulicFracturingWhitepaper2011.pdf>

Kelly, L. N. 2004. High Resolution Sequence Stratigraphy and Geochemistry of Middle and Upper Triassic Sedimentary Rocks, Northeast and Central Brooks Range, Alaska. MS thesis, University of Alaska Fairbanks.

Kupecz, J.A. 1995. Depositional Setting, Sequence Stratigraphy, Diagenesis, and Reservoir Potential of a Mixed-Lithology, Upwelling Deposit: The Upper Triassic Shublik Formation, Prudhoe Bay, Alaska. American Association of Petroleum Geologists Bulletin, v. 79, p. 1301-1319.

Manchanda, R., Roussel, N. P., Sharma, M. M. 2012. Factors Influencing Fracture Trajectories and Fracturing Pressure Data in a Horizontal Completion. Paper ARMA 12-633 presented at the US Rock Mechanics/Geomechanics Symposium, Chicago, IL.



Martin, R., Baihly, J., Malpani, R., Lindsay, G., Atwood, W.K. 2011. Understanding Production from Eagle Ford-Austin Chalk Systems. Paper SPE 145117 presented at the SPE Annual Technical Conference, Denver, CO.

Masters, J.A. 1979. Deep Basin Gas Trap, Western Canada. AAPG Bulletin 63, No. 2, 152.

Mohaghegh, S.D. 2013. A Critical View of Current State of Reservoir Modeling of Shale Assets. Paper SPE 165713 presented at the SPE Eastern Regional Meeting, Pittsburgh, PA.

Nolen, R. 2013. Elements of Hydraulic Fracturing. Schlumberger. [http://www.slb.com/~-/media/Files/resources/oilfield\\_review/ors13/sum13/defining\\_hydraulics.pdf](http://www.slb.com/~-/media/Files/resources/oilfield_review/ors13/sum13/defining_hydraulics.pdf)

Orangi, A., Nagarajan, N.R., Honarpour, M.M., Rosenzweig, J. 2011. Unconventional Shale Oil and Gas-Condensate Reservoir Production, Impact of Rock, Fluid, and Hydraulic Fractures. Paper SPE 140536 presented at the SPE Hydraulic Fracturing Technology Conference and Exhibition, The Woodlands, TX.

Osborn, S.G., Vengosh, A., Warner, N.R., Jackson, R.B. 2011. Methane Contamination of Drinking Water Accompanying Gas-Well Drilling and Hydraulic Fracturing. Proceedings of the National Academy of Sciences, USA. DOI: 10.1073/pnas.1100682108

Parrish, J.T., Whalen, M.T., Hulm, E.J. 2001. Shublik Formation Lithofacies, Environments, and Sequence Stratigraphy, Arctic Alaska, U.S.A. <http://www.webpages.uidaho.edu/~jparrish/NPRAShublik.pdf>

Peng, D. Y., Robinson, D. B. 1976. A New Two-Constant Equation of State. Industrial and Engineering Chemistry: Fundamentals 15: 59–64.

Rubin, B. 2010. Accurate Simulation of Non-Darcy Flow in Stimulated Fractured Shale Reservoirs. Paper SPE 132093 presented at the SPE Western Regional Meeting, Anaheim, CA.

Sondhi, M. 2011. Petrophysical Characterization of Eagle Ford Shale. MS thesis, University of Oklahoma.

Suchy, R.D., Newell K.D. 2011. Hydraulic Fracturing of Oil and Gas Wells in Kansas. Kansas Geological Survey Public Information Circular 32, <http://www.kgs.ku.edu/Publications/PIC/PIC32r1.pdf>

Tian, Y., Ayers, W., McCain, W. 2013. The Eagle Ford Shale Play, South Texas: Regional Variations in Fluid Types, Hydrocarbon Production and Reservoir Properties. Paper IPTC 16808 presented at the International Petroleum Technology Conference, Beijing, China.

Tivayanonda, V. 2012. Comparison of Single, Double, and Triple Linear Flow Models For Shale Gas/Oil Reservoirs. MS thesis, Texas A&M University.

Warpinski, N.R. 2009. Stress Amplification and Arch Dimensions in Proppant Beds Deposited by Waterfracs. Paper SPE 119350 presented at the SPE Hydraulic Fracturing Conference, The Woodlands, TX.

Wan, J., Barnum, R. S., DiGloria, D. C., Leahy-Dios, A., Missman, R., Hemphill, J. 2013. Factors Controlling Recovery in Liquids Rich Unconventional Systems. Paper IPTC 17103 presented at the International Petroleum Technology Conference, Beijing, China

Whitson, C.H. and Sunjerga, S. 2012. PVT in Liquid-Rich Shale Reservoirs. Paper SPE 155499 presented at the SPE Annual Technical Conference and Exhibition, San Antonio, TX.

Zanganeh, B., Ahmadi, M., Hanks, C., Awoleke, O. 2014. Proper Inclusion of Hydraulic Fracture and Unpropped Zone Conductivity and Fracturing Fluid Flowback in Single

Shale Oil Well Simulation. Paper SPE 169511 presented at the SPE Western North American and Rocky Mountain Joint Regional Meeting, Denver, CO.

Zhang, Z., Fassihi, M. R. 2013. Uncertainty Analysis and Assisted History Matching Workflow in Shale Oil Reservoirs. Paper SPE 168795 presented at the Unconventional Resources Technology Conference, Denver, CO.